

Measurement of Differential Branching Fractions of Inclusive $B \rightarrow X_u \ell^+ \nu_\ell$ Decays

L. Cao,^{1,*} W. Sutcliffe,¹ R. Van Tonder,¹ F. U. Bernlochner,^{1,†} I. Adachi,^{18,14} H. Aihara,⁸³ D. M. Asner,³ T. Aushev,²⁰ V. Babu,⁸ S. Bahinipati,²⁴ P. Behera,²⁶ K. Belous,³⁰ J. Bennett,⁵⁴ M. Bessner,¹⁷ T. Bilka,⁵ J. Biswal,³⁵ A. Bobrov,^{4,63} M. Bračko,^{51,35} P. Branchini,³² T. E. Browder,¹⁷ A. Budano,³² M. Campajola,^{31,56} D. Červenkov,⁵ M.-C. Chang,¹⁰ P. Chang,⁵⁹ B. G. Cheon,¹⁶ K. Chilikin,⁴⁵ H. E. Cho,¹⁶ K. Cho,⁴⁰ S.-J. Cho,⁹⁰ Y. Choi,⁷⁶ S. Choudhury,²⁵ D. Cinabro,⁸⁸ S. Cunliffe,⁸ T. Czank,³⁷ N. Dash,²⁶ G. De Pietro,³² R. Dhamija,²⁵ F. Di Capua,^{31,56} J. Dingfelder,¹ Z. Doležal,⁵ T. V. Dong,¹¹ S. Dubey,¹⁷ D. Epifanov,^{4,63} T. Ferber,⁸ D. Ferlewicz,⁵³ A. Frey,¹³ B. G. Fulsom,⁶⁵ R. Garg,⁶⁶ V. Gaur,⁸⁷ N. Gabyshev,^{4,63} A. Garmash,^{4,63} A. Giri,²⁵ P. Goldenzweig,³⁶ T. Gu,⁶⁸ K. Gudkova,^{4,63} S. Halder,⁷⁸ T. Hara,^{18,14} O. Hartbrich,¹⁷ K. Hayasaka,⁶² M. Hernandez Villanueva,⁸ W.-S. Hou,⁵⁹ C.-L. Hsu,⁷⁷ K. Inami,⁵⁵ A. Ishikawa,^{18,14} R. Itoh,^{18,14} M. Iwasaki,⁶⁴ W. W. Jacobs,²⁷ E.-J. Jang,¹⁵ S. Jia,¹¹ Y. Jin,⁸³ K. K. Joo,⁶ J. Kahn,³⁶ K. H. Kang,⁴³ H. Kichimi,¹⁸ C. Kiesling,⁵² C. H. Kim,¹⁶ D. Y. Kim,⁷⁵ S. H. Kim,⁷³ Y.-K. Kim,⁹⁰ T. D. Kimmel,⁸⁷ K. Kinoshita,⁷ P. Kodyš,⁵ T. Konno,³⁹ A. Korobov,^{4,63} S. Korpar,^{51,35} E. Kovalenko,^{4,63} P. Križan,^{47,35} R. Kroeger,⁵⁴ P. Krokovny,^{4,63} T. Kuhr,⁴⁸ R. Kulasiri,³⁸ M. Kumar,⁵⁰ R. Kumar,⁶⁹ K. Kumara,⁸⁸ A. Kuzmin,^{4,63} Y.-J. Kwon,⁹⁰ S. C. Lee,⁴³ C. H. Li,⁴⁶ J. Li,⁴³ L. K. Li,⁷ Y. B. Li,⁶⁷ L. Li Gioi,⁵² J. Libby,²⁶ K. Lieret,⁴⁸ D. Liventsev,^{88,18} C. MacQueen,⁵³ M. Masuda,^{82,70} M. Merola,^{31,56} F. Metzner,³⁶ K. Miyabayashi,⁵⁷ R. Mizuk,^{45,20} G. B. Mohanty,⁷⁸ S. Mohanty,^{78,86} M. Mrvar,²⁹ M. Nakao,^{18,14} A. Natochii,¹⁷ L. Nayak,²⁵ M. Niiyama,⁴² N. K. Nisar,³ S. Nishida,^{18,14} K. Nishimura,¹⁷ S. Ogawa,⁸⁰ H. Ono,^{61,62} Y. Onuki,⁸³ P. Oskin,⁴⁵ G. Pakhlova,^{20,45} S. Pardi,³¹ H. Park,⁴³ S.-H. Park,¹⁸ A. Passeri,³² S. Patra,²³ S. Paul,^{79,52} T. K. Pedlar,⁴⁹ L. E. Piilonen,⁸⁷ T. Podobnik,^{47,35} V. Popov,²⁰ E. Prencipe,²¹ M. T. Prim,¹ M. Röhrken,⁸ A. Rostomyan,⁸ N. Rout,²⁶ M. Rozanska,⁶⁰ G. Russo,⁵⁶ D. Sahoo,⁷⁸ S. Sandilya,²⁵ A. Sangal,⁷ L. Santelj,^{47,35} T. Sanuki,⁸¹ V. Savinov,⁶⁸ G. Schnell,^{2,22} J. Schueler,¹⁷ C. Schwanda,²⁹ A. J. Schwartz,⁷ Y. Seino,⁶² K. Senyo,⁸⁹ M. E. Sevier,⁵³ M. Shapkin,³⁰ C. Sharma,⁵⁰ C. P. Shen,¹¹ J.-G. Shiu,⁵⁹ B. Shwartz,^{4,63} F. Simon,⁵² A. Sokolov,³⁰ E. Solovieva,⁴⁵ M. Starič,³⁵ J. F. Strube,⁶⁵ M. Sumihama,¹² T. Sumiyoshi,⁸⁵ M. Takizawa,^{74,19,71} U. Tamponi,³³ K. Tanida,³⁴ Y. Tao,⁹ F. Tenchini,⁸ K. Trabelsi,⁴⁴ M. Uchida,⁸⁴ T. Uglov,^{45,20} S. Uno,^{18,14} P. Urquijo,⁵³ S. E. Vahsen,¹⁷ G. Varner,¹⁷ K. E. Varvell,⁷⁷ E. Waheed,¹⁸ C. H. Wang,⁵⁸ E. Wang,⁶⁸ M.-Z. Wang,⁵⁹ P. Wang,²⁸ X. L. Wang,¹¹ M. Watanabe,⁶² S. Watanuki,⁴⁴ O. Werbycka,⁶⁰ E. Won,⁴¹ B. D. Yabsley,⁷⁷ W. Yan,⁷² S. B. Yang,⁴¹ H. Ye,⁸ J. H. Yin,⁴¹ Z. P. Zhang,⁷² V. Zhilich,^{4,63} and V. Zhukova⁴⁵

(The Belle Collaboration)

¹University of Bonn, 53115 Bonn²Department of Physics, University of the Basque Country UPV/EHU, 48080 Bilbao³Brookhaven National Laboratory, Upton, New York 11973⁴Budker Institute of Nuclear Physics SB RAS, Novosibirsk 630090⁵Faculty of Mathematics and Physics, Charles University, 121 16 Prague⁶Chonnam National University, Gwangju 61186⁷University of Cincinnati, Cincinnati, Ohio 45221⁸Deutsches Elektronen-Synchrotron, 22607 Hamburg⁹University of Florida, Gainesville, Florida 32611¹⁰Department of Physics, Fu Jen Catholic University, Taipei 24205¹¹Key Laboratory of Nuclear Physics and Ion-beam Application (MOE)

and Institute of Modern Physics, Fudan University, Shanghai 200443

¹²Gifu University, Gifu 501-1193¹³II. Physikalisches Institut, Georg-August-Universität Göttingen, 37073 Göttingen¹⁴SOKENDAI (The Graduate University for Advanced Studies), Hayama 240-0193¹⁵Gyeongsang National University, Jinju 52828¹⁶Department of Physics and Institute of Natural Sciences, Hanyang University, Seoul 04763¹⁷University of Hawaii, Honolulu, Hawaii 96822¹⁸High Energy Accelerator Research Organization (KEK), Tsukuba 305-0801¹⁹J-PARC Branch, KEK Theory Center, High Energy Accelerator Research Organization (KEK), Tsukuba 305-0801²⁰National Research University Higher School of Economics, Moscow 101000²¹Forschungszentrum Jülich, 52425 Jülich²²IKERBASQUE, Basque Foundation for Science, 48013 Bilbao²³Indian Institute of Science Education and Research Mohali, SAS Nagar, 140306²⁴Indian Institute of Technology Bhubaneswar, Satya Nagar 751007²⁵Indian Institute of Technology Hyderabad, Telangana 502285²⁶Indian Institute of Technology Madras, Chennai 600036²⁷Indiana University, Bloomington, Indiana 47408

- ²⁸*Institute of High Energy Physics, Chinese Academy of Sciences, Beijing 100049*
- ²⁹*Institute of High Energy Physics, Vienna 1050*
- ³⁰*Institute for High Energy Physics, Protvino 142281*
- ³¹*INFN - Sezione di Napoli, I-80126 Napoli*
- ³²*INFN - Sezione di Roma Tre, I-00146 Roma*
- ³³*INFN - Sezione di Torino, I-10125 Torino*
- ³⁴*Advanced Science Research Center, Japan Atomic Energy Agency, Naka 319-1195*
- ³⁵*J. Stefan Institute, 1000 Ljubljana*
- ³⁶*Institut für Experimentelle Teilchenphysik, Karlsruher Institut für Technologie, 76131 Karlsruhe*
- ³⁷*Kavli Institute for the Physics and Mathematics of the Universe (WPI), University of Tokyo, Kashiwa 277-8583*
- ³⁸*Kennesaw State University, Kennesaw, Georgia 30144*
- ³⁹*Kitasato University, Sagami-hara 252-0373*
- ⁴⁰*Korea Institute of Science and Technology Information, Daejeon 34141*
- ⁴¹*Korea University, Seoul 02841*
- ⁴²*Kyoto Sangyo University, Kyoto 603-8555*
- ⁴³*Kyungpook National University, Daegu 41566*
- ⁴⁴*Université Paris-Saclay, CNRS/IN2P3, IJCLab, 91405 Orsay*
- ⁴⁵*P.N. Lebedev Physical Institute of the Russian Academy of Sciences, Moscow 119991*
- ⁴⁶*Liaoning Normal University, Dalian 116029*
- ⁴⁷*Faculty of Mathematics and Physics, University of Ljubljana, 1000 Ljubljana*
- ⁴⁸*Ludwig Maximilians University, 80539 Munich*
- ⁴⁹*Luther College, Decorah, Iowa 52101*
- ⁵⁰*Malaviya National Institute of Technology Jaipur, Jaipur 302017*
- ⁵¹*Faculty of Chemistry and Chemical Engineering, University of Maribor, 2000 Maribor*
- ⁵²*Max-Planck-Institut für Physik, 80805 München*
- ⁵³*School of Physics, University of Melbourne, Victoria 3010*
- ⁵⁴*University of Mississippi, University, Mississippi 38677*
- ⁵⁵*Graduate School of Science, Nagoya University, Nagoya 464-8602*
- ⁵⁶*Università di Napoli Federico II, I-80126 Napoli*
- ⁵⁷*Nara Women's University, Nara 630-8506*
- ⁵⁸*National United University, Miao Li 36003*
- ⁵⁹*Department of Physics, National Taiwan University, Taipei 10617*
- ⁶⁰*H. Niewodniczanski Institute of Nuclear Physics, Krakow 31-342*
- ⁶¹*Nippon Dental University, Niigata 951-8580*
- ⁶²*Niigata University, Niigata 950-2181*
- ⁶³*Novosibirsk State University, Novosibirsk 630090*
- ⁶⁴*Osaka City University, Osaka 558-8585*
- ⁶⁵*Pacific Northwest National Laboratory, Richland, Washington 99352*
- ⁶⁶*Panjab University, Chandigarh 160014*
- ⁶⁷*Peking University, Beijing 100871*
- ⁶⁸*University of Pittsburgh, Pittsburgh, Pennsylvania 15260*
- ⁶⁹*Punjab Agricultural University, Ludhiana 141004*
- ⁷⁰*Research Center for Nuclear Physics, Osaka University, Osaka 567-0047*
- ⁷¹*Meson Science Laboratory, Cluster for Pioneering Research, RIKEN, Saitama 351-0198*
- ⁷²*Department of Modern Physics and State Key Laboratory of Particle Detection and Electronics, University of Science and Technology of China, Hefei 230026*
- ⁷³*Seoul National University, Seoul 08826*
- ⁷⁴*Showa Pharmaceutical University, Tokyo 194-8543*
- ⁷⁵*Soongsil University, Seoul 06978*
- ⁷⁶*Sungkyunkwan University, Suwon 16419*
- ⁷⁷*School of Physics, University of Sydney, New South Wales 2006*
- ⁷⁸*Tata Institute of Fundamental Research, Mumbai 400005*
- ⁷⁹*Department of Physics, Technische Universität München, 85748 Garching*
- ⁸⁰*Toho University, Funabashi 274-8510*
- ⁸¹*Department of Physics, Tohoku University, Sendai 980-8578*
- ⁸²*Earthquake Research Institute, University of Tokyo, Tokyo 113-0032*
- ⁸³*Department of Physics, University of Tokyo, Tokyo 113-0033*
- ⁸⁴*Tokyo Institute of Technology, Tokyo 152-8550*
- ⁸⁵*Tokyo Metropolitan University, Tokyo 192-0397*
- ⁸⁶*Utkal University, Bhubaneswar 751004*
- ⁸⁷*Virginia Polytechnic Institute and State University, Blacksburg, Virginia 24061*
- ⁸⁸*Wayne State University, Detroit, Michigan 48202*
- ⁸⁹*Yamagata University, Yamagata 990-8560*
- ⁹⁰*Yonsei University, Seoul 03722*

(Dated: June 22, 2022)

The first measurements of differential branching fractions of inclusive semileptonic $B \rightarrow X_u \ell^+ \nu_\ell$ decays are performed using the full Belle data set of 711 fb^{-1} of integrated luminosity at the $\Upsilon(4S)$ resonance and for $\ell = e, \mu$. Differential branching fractions are reported as a function of the lepton momentum, the four-momentum-transfer squared, light-cone momenta, the hadronic mass, and the hadronic mass squared. They are obtained by subtracting the backgrounds from semileptonic $B \rightarrow X_c \ell^+ \nu_\ell$ decays and other processes, and corrected for resolution and acceptance effects. The measured distributions are compared to predictions from inclusive and hybrid $B \rightarrow X_u \ell^+ \nu_\ell$ calculations.

PACS numbers: 12.15.Hh, 13.20.-v, 14.40.Nd

In this Letter we present measurements of the differential branching fractions of inclusive semileptonic $B \rightarrow X_u \ell^+ \nu_\ell$ decays¹, obtained from analyzing the full Belle data set of 711 fb^{-1} of integrated luminosity at the $\Upsilon(4S)$ resonance and for $\ell = e, \mu$. The measured distributions can be used for future studies of the non-perturbative decay dynamics of $B \rightarrow X_u \ell^+ \nu_\ell$ transitions, and novel determinations of the b -quark mass m_b and of the CKM matrix element $|V_{ub}|$. The presented measurements use the same collision events that were analyzed in Ref. [1]. Therein, partial branching fractions of charmless semileptonic decays were reported using an analysis technique relying on the full reconstruction of the second B meson of the $e^+ e^- \rightarrow \Upsilon(4S) \rightarrow B\bar{B}$ process. This approach allows for the direct reconstruction of the four-momentum of the hadronic X system of the $B \rightarrow X_u \ell^+ \nu_\ell$ process and other kinematic quantities of interest. The analysis strategy of the presented measurements follows Ref. [1] closely, but additional selection criteria are applied to improve the resolution of key variables and further suppress backgrounds from $B \rightarrow X_c \ell^+ \nu_\ell$ decays and other processes.

Differential branching fractions are reported as a function of the lepton energy in the signal B rest frame E_ℓ^B , the invariant mass M_X and mass squared M_X^2 of the hadronic X system, the four-momentum-transfer squared $q^2 = (p_B - p_X)^2$ of the B to the lepton and neutrino system, and the two light-cone momenta $P_\pm = (E_X \mp |\mathbf{p}_X|)$ with E_X and \mathbf{p}_X in the signal B rest frame. Measurements of these distributions are of great interest as they allow for the study of non-perturbative shape functions [2]. Shape functions describes the Fermi motion of the b quark inside the B meson, and enter in the calculation of the dynamics of $B \rightarrow X_u \ell^+ \nu_\ell$ decays. Currently, properties of the leading-order Λ_{QCD}/m_b shape function can only be studied using the photon energy spectrum of $B \rightarrow X_s \gamma$ decays and moments of the lepton energy or hadronic invariant mass in charmed semileptonic B decays [3–5]. The modeling of both the leading and sub-leading shape functions introduce large theory uncertain-

ties on predictions of the $B \rightarrow X_u \ell^+ \nu_\ell$ decay rate, and hence on the determination of $|V_{ub}|$. With the presented differential branching fractions, we provide the necessary experimental input for future model-independent approaches, whose aim is to reduce this model dependence by directly measuring the shape function [6, 7].

We analyze $(772 \pm 10) \times 10^6$ B meson pairs recorded at the $\Upsilon(4S)$ resonance energy and 79 fb^{-1} of collision events recorded 60 MeV below the $\Upsilon(4S)$ peak, which were both recorded at the KEKB e^+e^- collider [8] by the Belle detector. Belle is a large-solid-angle magnetic spectrometer and a detailed description of its sub-detectors and performance can be found in Ref. [9]. Monte Carlo (MC) samples of B meson decays and continuum processes ($e^+e^- \rightarrow q\bar{q}$ with $q = u, d, s, c$) are simulated using the EvtGen generator [10] and a detailed description of all samples and models is given in Ref. [1]. The simulated samples are used for the background subtraction and to correct for detector resolution, selection, and acceptance effects. The sample sizes used correspond to approximately ten and five times, respectively, the Belle collision data for B meson production and continuum processes. Semileptonic $B \rightarrow X_u \ell^+ \nu_\ell$ decays are modeled as a mixture of specific exclusive modes and non-resonant

TABLE I. Semileptonic $B \rightarrow X_u \ell^+ \nu_\ell$ decays are modeled as a mixture of specific exclusive modes and non-resonant contributions. The branching fractions are from the world averages from Ref. [11] and the models and form factors (FFs) used are listed. We use natural units ($\hbar = c = 1$).

B	Value B^+	Value B^0
$B \rightarrow \pi \ell^+ \nu_\ell$ ^{a,e}	$(7.8 \pm 0.3) \times 10^{-5}$	$(1.5 \pm 0.06) \times 10^{-4}$
$B \rightarrow \eta \ell^+ \nu_\ell$ ^{b,e}	$(3.9 \pm 0.5) \times 10^{-5}$	-
$B \rightarrow \eta' \ell^+ \nu_\ell$ ^{b,e}	$(2.3 \pm 0.8) \times 10^{-5}$	-
$B \rightarrow \omega \ell^+ \nu_\ell$ ^{c,e}	$(1.2 \pm 0.1) \times 10^{-4}$	-
$B \rightarrow \rho \ell^+ \nu_\ell$ ^{c,e}	$(1.6 \pm 0.1) \times 10^{-4}$	$(2.9 \pm 0.2) \times 10^{-4}$
$B \rightarrow X_u \ell^+ \nu_\ell$ ^{d,e}	$(2.2 \pm 0.3) \times 10^{-3}$	$(2.0 \pm 0.3) \times 10^{-3}$

^a BCL FFs [12] from fit to LQCD [13] and Ref. [14]

^b Pole FFs from LCSR [15]

^c BSZ FFs fit [16] to LCSR [17] and Refs. [18–20]

^d DFN [21] ($m_b^{\text{KN}} = (4.66 \pm 0.04) \text{ GeV}$, $a^{\text{KN}} = 1.3 \pm 0.5$) or BLNP model [22] ($m_b^{\text{SF}} = 4.61 \text{ GeV}$, $\mu_\pi^{\text{SF}} = 0.20 \text{ GeV}^2$)

^e Incl. and excl. decays are mixed using hybrid approach [23]

¹ Charge conjugation is implied and $B \rightarrow X_u \ell^+ \nu_\ell$ is defined as the average branching fraction of B^+ and B^0 meson decays.

contributions using a so-called ‘hybrid’ approach [23], following closely the implementation of [24, 25]. In the hybrid approach, the triple differential rate of the inclusive and combined exclusive predictions are combined such that partial rates of the inclusive prediction are recovered. This is achieved by assigning three dimensional weights to the inclusive contribution as a function of the generator-level q^2 , E_ℓ^B , and M_X . For the inclusive contribution we use two different calculations [21, 22] and treat their difference as a systematic uncertainty. The simulated inclusive $B \rightarrow X_u \ell^+ \nu_\ell$ events are hadronized with the JETSET algorithm [26] into final states with two or more mesons. A summary of the used $B \rightarrow X_u \ell^+ \nu_\ell$ branching fractions and decay models is given in Table I. Semileptonic $B \rightarrow X_c \ell^+ \nu_\ell$ decays are dominated by $B \rightarrow D \ell^+ \nu_\ell$ and $B \rightarrow D^* \ell^+ \nu_\ell$ decays, which are simulated with form factor parametrizations discussed in Refs. [27–29] and values determined by Refs. [30, 31]. The remaining $B \rightarrow X_c \ell^+ \nu_\ell$ decays are simulated as a mix of resonant and non-resonant modes, using Ref. [32] for the modeling of $B \rightarrow D^{**} \ell^+ \nu_\ell$ form factors. The known difference between inclusive and the sum of measured exclusive $B \rightarrow X_c \ell^+ \nu_\ell$ is filled with $B \rightarrow D^{(*)} \eta \ell^+ \nu_\ell$ decays.

Collision events are reconstructed using the multivariate algorithm of Ref. [33], in which one of the two B mesons is fully reconstructed in hadronic final states (labeled as B_{tag}). Signal candidates are reconstructed by identifying an electron or muon candidate with $E_\ell^B = |\mathbf{p}_\ell^B| > 1 \text{ GeV}$ in the signal B rest frame, and by reconstructing the hadronic X system of the $B \rightarrow X_u \ell^+ \nu_\ell$ semileptonic process using charged particles and neutral energy depositions of the collision event not used in the reconstruction of the B_{tag} candidate. The largest background after the reconstruction is from the CKM-favored $B \rightarrow X_c \ell^+ \nu_\ell$ process, which possesses a very similar decay signature, completely dominating the selected candidate events. To identify $B \rightarrow X_u \ell^+ \nu_\ell$ candidates, eleven distinguishing features are combined into a single discriminant using a multivariate classifier in the form of boosted decision trees (BDTs) using the implementation of Ref. [34]. The most discriminating variables are the reconstructed neutrino mass, M_{miss}^2 , the vertex fit probability of the $X\ell$ decay vertex, and the number of identified K^\pm and K_S^0 in the X system. To improve the resolution on the reconstructed variables or the signal to background ratio, additional selections are applied. For the measurements involving the hadronic X system (M_X , M_X^2 , q^2 , P_\pm), we demand the missing energy, E_{miss} , and the magnitude of the missing momentum, $|\mathbf{p}_{\text{miss}}|$, of the collision to be consistent with each other by requiring $|E_{\text{miss}} - |\mathbf{p}_{\text{miss}}|| < 0.1 \text{ GeV}$. This improves the resolution by 21–37%, depending on the observable, and removes poorly reconstructed events. The signal efficiency after the BDT selection and this additional requirement is 8% whilst rejecting 99.5% of all

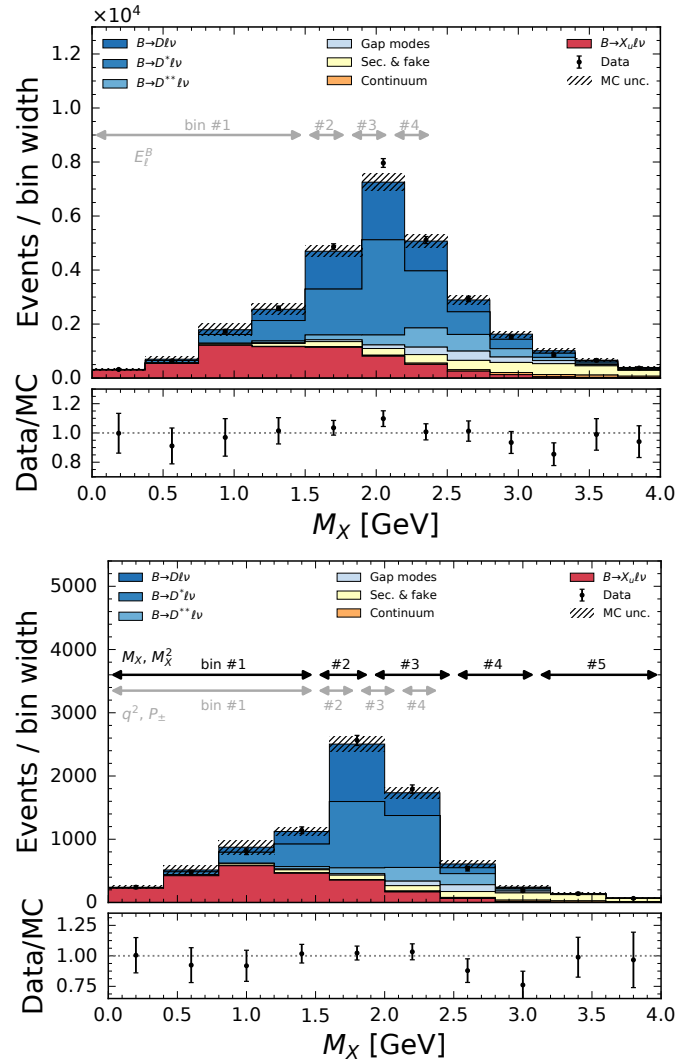


FIG. 1. The reconstructed M_X distributions after the BDT selection without (top) and with (bottom) the requirement of $|E_{\text{miss}} - |\mathbf{p}_{\text{miss}}|| < 0.1 \text{ GeV}$ are shown. The arrows indicate the coarse binning used in the background subtraction fit for the different variables. Removing the $M_X > 2.4 \text{ GeV}$ events improves the signal to background ratio for E_ℓ^B , q^2 , and P_\pm , but is not necessary for measurements of M_X and M_X^2 .

$B \rightarrow X_c \ell^+ \nu_\ell$ background events, as defined with respect to all selected signal or $B \rightarrow X_c \ell^+ \nu_\ell$ events after successfully identifying a suitable B_{tag} candidate. To reduce the contamination of $B \rightarrow X_c \ell^+ \nu_\ell$ and other backgrounds, for the measurements of q^2 and the light-cone momenta P_\pm , an additional requirement of $M_X < 2.4 \text{ GeV}$ is imposed: this selection, mostly targeting poorly understood high-mass X_c states, removes in addition background from secondary leptons and reduces the $B \rightarrow X_c \ell^+ \nu_\ell$ contamination by an additional 20%. The reconstruction resolution of the lepton energy is excellent, thus no requirement on the missing energy and the magnitude of the missing momentum of the event is imposed,

but to reduce background contributions we also require $M_X < 2.4$ GeV. This results in a signal efficiency of 17% and 99% of $B \rightarrow X_c \ell^+ \nu_\ell$ background events are rejected as defined with respect to all events after the B_{tag} selection.

The differential branching fractions are extracted by subtracting the remaining background contributions from $B \rightarrow X_c \ell^+ \nu_\ell$ and other sources in the measured distributions. This is implemented in a four-step procedure: first a binned likelihood fit to the M_X distribution is carried out to estimate the number of background events. The M_X fit takes the shape of signal and background from MC simulations and includes as nuisance parameters systematic effects that can impact the template shapes. To reduce the dependence on the precise modeling of the $B \rightarrow X_u \ell^+ \nu_\ell$ process, a coarse binning is used. In particular, the resonance region ($M_X \in [0, 1.5]$ GeV) is described by a single bin. The analyzed hadronic invariant mass spectra with and without the selection on $|E_{\text{miss}} - |\mathbf{p}_{\text{miss}}|| < 0.1$ GeV and the used binning for the different fits are shown in Figure 1.

In the second step, the background is subtracted using the estimated normalization from the corresponding M_X fit in the kinematic variable under study. The background shape is taken from MC simulation. The statistical uncertainty on the background subtracted yields are determined using a bootstrapping procedure [35, 36] to properly incorporate the correlation from the M_X fit as the same data events are analyzed. The same method is used to determine the statistical correlations between all bins of all measured distributions. The systematic uncertainties associated with modeling the background shape and normalization are also propagated into the uncertainties of the estimated signal yields. In the third step, the signal yields are unfolded using the SVD algorithm from Ref. [37] with the implementation of Ref. [38]. The regularization parameter of the unfolding method was carefully tuned with simulated samples to minimize the dependence on m_b , the shape function modeling, and the composition of the $B \rightarrow X_u \ell^+ \nu_\ell$ signal. In the final step the unfolded yields are corrected for efficiency and acceptance effects to the partial phase space defined by $E_\ell^B > 1$ GeV, also correcting for QED final-state radiation. The full analysis procedure was validated with independent MC samples and ensembles of pseudo-experiments and no biases of central values or uncertainties were observed.

Systematic uncertainties from the background subtraction, the modeling of the detector response for $B \rightarrow X_u \ell^+ \nu_\ell$, and uncertainties entering the total normalization are consistently propagated through the background subtraction, unfolding, and efficiency correction procedure. For the background subtraction we evaluate $B \rightarrow X_u \ell^+ \nu_\ell$ and $B \rightarrow X_c \ell^+ \nu_\ell$ modeling (FFs, non-perturbative parameters and composition) and detector related systematic uncertainties. The largest systematic

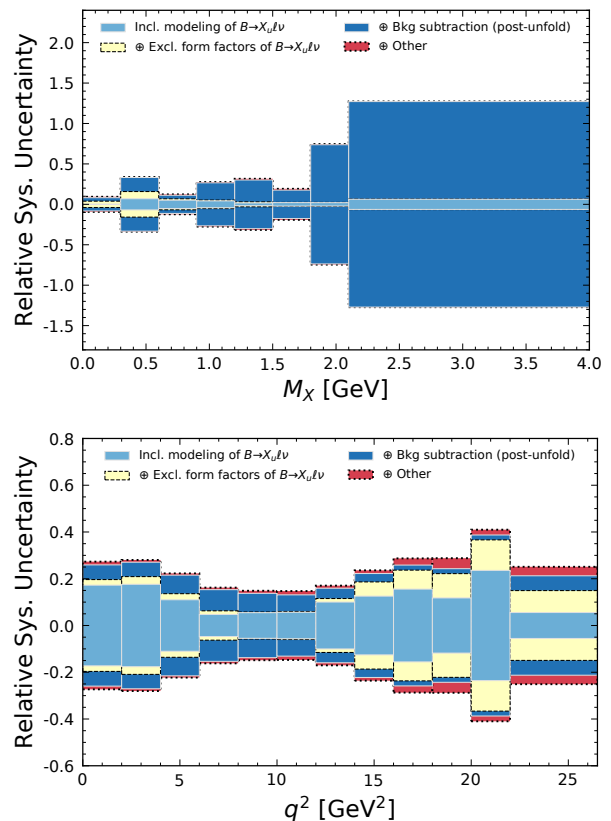


FIG. 2. The relative systematic uncertainties on the unfolded differential branching fraction as a function of M_X and q^2 are shown. The different uncertainty sources are color coded.

uncertainties are typically from the assumptions entering the modeling of the $B \rightarrow X_u \ell^+ \nu_\ell$ signal composition, but depending on the region of phase space also the background subtraction uncertainty can be a dominant source of uncertainty. Figure 2 shows the relative uncertainties on the unfolded differential branching fractions as a function of M_X and q^2 . The total systematic uncertainties range from 9 to 130% in relative error, and the background uncertainty is the dominant source of error in regions of phase space that are enriched in $B \rightarrow X_c \ell^+ \nu_\ell$ (e.g. above $M_X \approx m_{D^0} = 1.86$ GeV). The exclusive $B \rightarrow X_u \ell^+ \nu_\ell$ modeling errors only contribute significantly in the resonance region at low M_X or high q^2 . The full systematic and statistical correlations between all measured distributions is determined to allow for a future simultaneous analysis of all measured distributions, and is provided with the full systematic uncertainties of all measured distributions in Ref. [39].

The measured differential branching fractions as a function of E_ℓ^B , q^2 , M_X , M_X^2 , P_- , and P_+ are shown in Figure 3 and the numerical values with full correlations can be found in Ref. [39]. The distributions are compared to the $B \rightarrow X_u \ell^+ \nu_\ell$ hybrid MC and the fully inclusive DFN [21] and BLNP [40] predictions with model

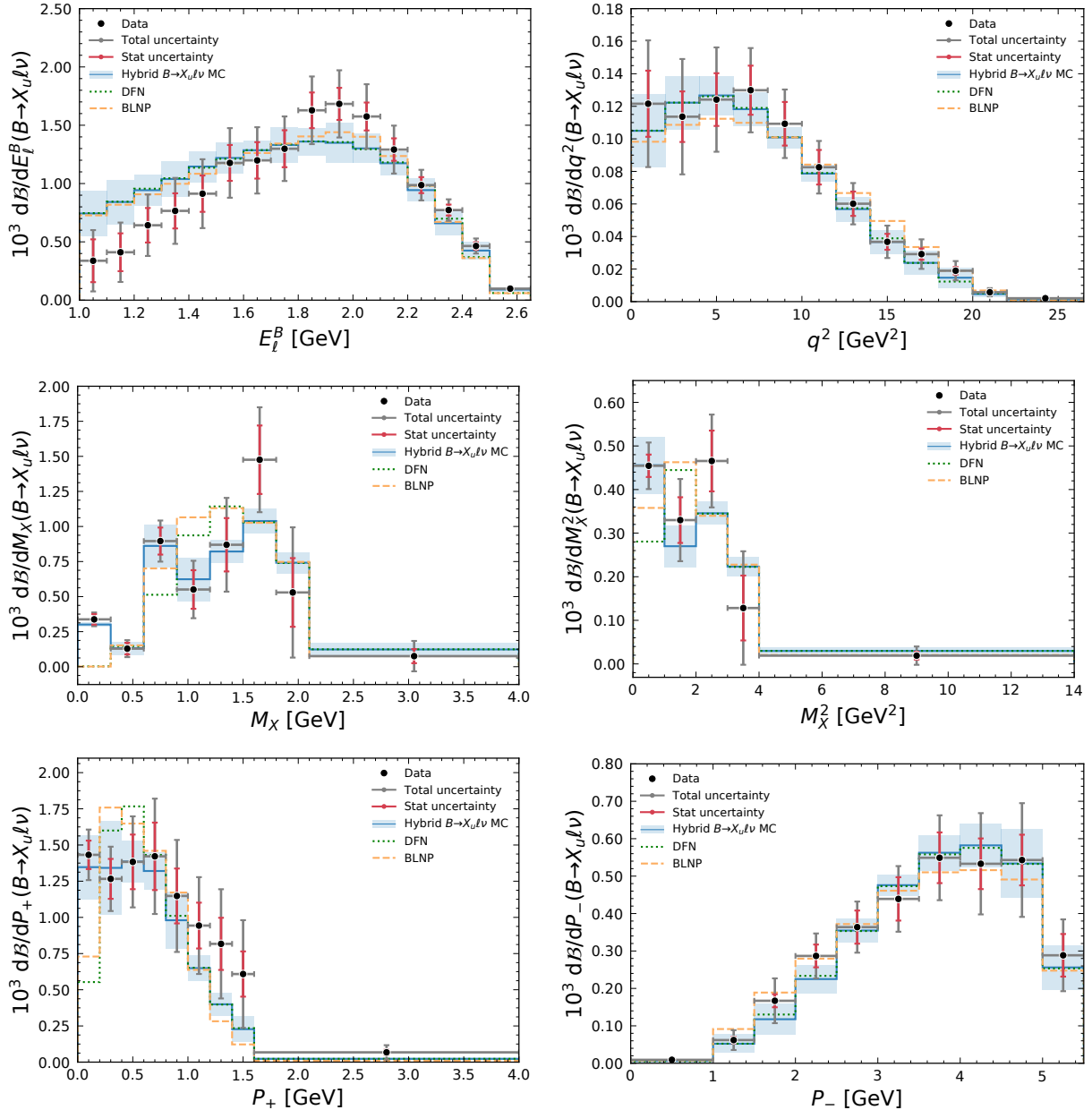


FIG. 3. The measured differential $B \rightarrow X_u \ell^+ \nu_\ell$ branching fractions are shown: the lepton energy in the B rest frame (E_ℓ^B), the four-momentum-transfer squared of the B to the X_u system ($q^2 = (p_B - p_X)^2$), the invariant hadronic mass and mass squared of the X_u system (M_X , M_X^2), and the light-cone momenta of the hadronic X_u system ($P_\pm = (E_X \mp |\mathbf{p}_X|)$). The hybrid MC prediction and two inclusive calculations are also shown and scaled to $\Delta\mathcal{B} = 1.59 \times 10^{-3}$.

parameters listed in Table I. All predictions are scaled to match the $B \rightarrow X_u \ell^+ \nu_\ell$ partial branching fraction ($\Delta\mathcal{B}$) with $E_\ell^B > 1$ GeV of $\Delta\mathcal{B} = 1.59 \times 10^{-3}$ from Ref. [1]. The uncertainty band of the hybrid prediction includes variations on the composition, form factors, and the inclusive modeling, whose central value is based on the DFN prediction but includes the difference to BLNP as an additional uncertainty. The agreement between the measured and predicted distributions is fair overall, with differences occurring for the fully inclusive predictions in

the resonance region of, e.g., low M_X , and near the end-point of q^2 and E_ℓ^B . There the hybrid MC describes the $B \rightarrow X_u \ell^+ \nu_\ell$ process more adequately due to the explicit inclusion of resonant contributions. The largest discrepancy is observed in E_ℓ^B , but the data points ranging of $E_\ell^B \in [1 - 1.8]$ GeV exhibit strong correlations and are only weakly correlated or anti-correlated with the other bins of the spectrum.

In conclusion, this Letter presents the first measurements of differential branching fractions of inclusive

semileptonic $B \rightarrow X_u \ell^+ \nu_\ell$ decays as a function of E_ℓ^B , q^2 , M_X , M_X^2 , P_- , and P_+ (a first preliminary measurement of the shape of the spectrum of M_X^2 was presented in Ref. [41] and Ref. [42] reported a differential branching fraction measurement as a function E_e^B , but without providing the full experimental uncertainties). The measurements use the full Belle data set of 711 fb^{-1} of integrated luminosity at the $\Upsilon(4S)$ resonance and for $\ell = e, \mu$ in which one of the two B mesons was fully reconstructed in hadronic modes. The differential branching fractions are obtained by subtracting $B \rightarrow X_c \ell^+ \nu_\ell$ and other backgrounds with the normalization determined by a fit to the M_X distribution of the hadronic X system. The resulting distributions are corrected for detector resolution and efficiency effects and unfolded to the phase space of the lepton energy of $E_\ell^B > 1 \text{ GeV}$ in the rest frame of the signal B meson. The measurements are, depending on the region of phase space, statistically or systematically limited, and show fair agreement to hybrid and inclusive predictions of $B \rightarrow X_u \ell^+ \nu_\ell$ decays. The measured distributions are sensitive to the shape-function governing the non-perturbative dynamics of the $b \rightarrow u$ transition and will allow future direct determinations of the shape-function and $|V_{ub}|$, as proposed by Refs. [6, 7].

We thank Kerstin Tackmann, Frank Tackmann, Zoltan Ligeti, and Dean Robinson for discussions about the content of this manuscript. LC, WS, RvT, and FB were supported by the German Research Foundation (DFG) Emmy-Noether Grant No. BE 6075/1-1. We thank the KEKB group for the excellent operation of the accelerator; the KEK cryogenics group for the efficient operation of the solenoid; and the KEK computer group, and the Pacific Northwest National Laboratory (PNNL) Environmental Molecular Sciences Laboratory (EMSL) computing group for strong computing support; and the National Institute of Informatics, and Science Information NETwork 5 (SINET5) for valuable network support. We acknowledge support from the Ministry of Education, Culture, Sports, Science, and Technology (MEXT) of Japan, the Japan Society for the Promotion of Science (JSPS), and the Tau-Lepton Physics Research Center of Nagoya University; the Australian Research Council including grants DP180102629, DP170102389, DP170102204, DP150103061, FT130100303; Austrian Federal Ministry of Education, Science and Research (FWF) and FWF Austrian Science Fund No. P 31361-N36; the National Natural Science Foundation of China under Contracts No. 11435013, No. 11475187, No. 11521505, No. 11575017, No. 11675166, No. 11705209; Key Research Program of Frontier Sciences, Chinese Academy of Sciences (CAS), Grant No. QYZDJ-SSW-SLH011; the CAS Center for Excellence in Particle Physics (CCEPP); the Shanghai Pujiang Program under Grant No. 18PJ1401000; the Shanghai Science and Technology Committee (STCSM) under Grant No. 19ZR1403000;

the Ministry of Education, Youth and Sports of the Czech Republic under Contract No. LTT17020; Horizon 2020 ERC Advanced Grant No. 884719 and ERC Starting Grant No. 947006 “InterLeptons” (European Union); the Carl Zeiss Foundation, the Deutsche Forschungsgemeinschaft, the Excellence Cluster Universe, and the VolkswagenStiftung; the Department of Atomic Energy (Project Identification No. RTI 4002) and the Department of Science and Technology of India; the Istituto Nazionale di Fisica Nucleare of Italy; National Research Foundation (NRF) of Korea Grant Nos. 2016R1D1A1B-01010135, 2016R1D1A1B02012900, 2018R1A2B3003643, 2018R1A6A1A06024970, 2018R1D1A1B07047294, 2019K1A3A7A09033840, 2019R1H1A3A01058933; Radiation Science Research Institute, Foreign Large-size Research Facility Application Supporting project, the Global Science Experimental Data Hub Center of the Korea Institute of Science and Technology Information and KREONET/GLORIAD; the Polish Ministry of Science and Higher Education and the National Science Center; the Ministry of Science and Higher Education of the Russian Federation, Agreement 14.W03.31.0026, and the HSE University Basic Research Program, Moscow; University of Tabuk research grants S-1440-0321, S-0256-1438, and S-0280-1439 (Saudi Arabia); the Slovenian Research Agency Grant Nos. J1-9124 and P1-0135; Ikerbasque, Basque Foundation for Science, Spain; the Swiss National Science Foundation; the Ministry of Education and the Ministry of Science and Technology of Taiwan; and the United States Department of Energy and the National Science Foundation.

* cao@physik.uni-bonn.de

† florian.bernlodner@uni-bonn.de

- [1] L. Cao *et al.* (Belle), *Phys. Rev. D* **104**, 012008 (2021), 2102.00020.
- [2] M. Neubert, *Phys. Rev. D* **49**, 3392 (1994), arXiv:hep-ph/9311325.
- [3] P. Gambino and N. Uraltsev, *Eur. Phys. J. C* **34**, 181 (2004), arXiv:hep-ph/0401063.
- [4] C. W. Bauer, Z. Ligeti, M. Luke, A. V. Manohar, and M. Trott, *Phys. Rev. D* **70**, 094017 (2004), arXiv:hep-ph/0408002.
- [5] D. Benson, I. I. Bigi, and N. Uraltsev, *Nucl. Phys. B* **710**, 371 (2005), arXiv:hep-ph/0410080.
- [6] F. U. Bernlochner, H. Lacker, Z. Ligeti, I. W. Stewart, F. J. Tackmann, and K. Tackmann (SIMBA Collaboration), (2020), arXiv:2007.04320 [hep-ph].
- [7] P. Gambino, K. J. Healey, and C. Mondino, *Phys. Rev. D* **94**, 014031 (2016), arXiv:1604.07598 [hep-ph].
- [8] S. Kurokawa and E. Kikutani, *Nucl. Instr. and Meth.* **A499**, 1 (2003), and other papers included in this Volume; T. Abe *et al.*, *Prog. Theor. Exp. Phys.* **2013**, 03A001 (2013) and references therein.
- [9] A. Abashian *et al.*, *Nucl. Instrum. Meth.* **A479**, 117 (2002), also see detector section in J. Brodzicka *et al.*,

- Prog. Theor. Exp. Phys. **2012**, 04D001 (2012).
- [10] D. J. Lange, *Nucl. Instr. and Meth. A* **462**, 152 (2001).
- [11] P. Zyla *et al.* (Particle Data Group), Prog. Theor. Exp. Phys. **2020** **083C01** (2020).
- [12] C. Bourrely, I. Caprini, and L. Lellouch, *Phys. Rev. D* **79**, 013008 (2009), [Erratum: *Phys. Rev. D* **82**, 099902 (2010)], [arXiv:0807.2722 \[hep-ph\]](#).
- [13] J. A. Bailey *et al.* (Fermilab Lattice and MILC Collaborations), *Phys. Rev. D* **92**, 014024 (2015), [arXiv:1503.07839 \[hep-lat\]](#).
- [14] Y. S. Amhis *et al.* (HFLAV), *Eur. Phys. J. C* **81**, 226 (2021), [arXiv:1909.12524 \[hep-ex\]](#).
- [15] G. Duplancic and B. Melic, *J. High Energy Phys.* **11**, 138 (2015), [arXiv:1508.05287 \[hep-ph\]](#).
- [16] F. U. Bernlochner, M. T. Prim, and D. J. Robinson, (2021), [arXiv:2104.05739 \[hep-ph\]](#).
- [17] A. Bharucha, *J. High Energy Phys.* **05**, 092 (2012), [arXiv:1203.1359 \[hep-ph\]](#).
- [18] A. Sibidanov *et al.* (Belle Collaboration), *Phys. Rev. D* **88**, 032005 (2013), [arXiv:1306.2781 \[hep-ex\]](#).
- [19] J. P. Lees *et al.* (BaBar Collaboration), *Phys. Rev. D* **87**, 032004 (2013), [Erratum: *Phys. Rev. D* **87**, 099904 (2013)], [arXiv:1205.6245 \[hep-ex\]](#).
- [20] P. del Amo Sanchez *et al.* (BaBar Collaboration), *Phys. Rev. D* **83**, 032007 (2011), [arXiv:1005.3288 \[hep-ex\]](#).
- [21] F. De Fazio and M. Neubert, *J. High Energy Phys.* **06**, 017 (1999), [arXiv:hep-ph/9905351 \[hep-ph\]](#).
- [22] B. O. Lange, M. Neubert, and G. Paz, *Phys. Rev. D* **72**, 073006 (2005), [arXiv:hep-ph/0504071](#).
- [23] C. Ramirez, J. F. Donoghue, and G. Burdman, *Phys. Rev. D* **41**, 1496 (1990).
- [24] M. Prim *et al.* (Belle Collaboration), *Phys. Rev. D* **101**, 032007 (2020), [arXiv:1911.03186 \[hep-ex\]](#).
- [25] M. Prim, “b2-hive/effort v0.1.0,” (2020).
- [26] T. Sjöstrand, *Comput. Phys. Commun.* **82**, 74 (1994).
- [27] C. G. Boyd, B. Grinstein, and R. F. Lebed, *Phys. Rev. Lett.* **74**, 4603 (1995), [arXiv:hep-ph/9412324 \[hep-ph\]](#).
- [28] B. Grinstein and A. Kobach, *Phys. Lett. B* **771**, 359 (2017), [arXiv:1703.08170 \[hep-ph\]](#).
- [29] D. Bigi, P. Gambino, and S. Schacht, *Phys. Lett. B* **769**, 441 (2017), [arXiv:1703.06124 \[hep-ph\]](#).
- [30] R. Glattauer *et al.* (Belle Collaboration), *Phys. Rev. D* **93**, 032006 (2016), [arXiv:1510.03657 \[hep-ex\]](#).
- [31] E. Waheed *et al.* (Belle Collaboration), *Phys. Rev. D* **100**, 052007 (2019), [arXiv:1809.03290 \[hep-ex\]](#).
- [32] F. U. Bernlochner and Z. Ligeti, *Phys. Rev. D* **95**, 014022 (2017), [arXiv:1606.09300 \[hep-ph\]](#).
- [33] M. Feindt, F. Keller, M. Kreps, T. Kuhr, S. Neubauer, D. Zander, and A. Zupanc, *Nucl. Instrum. Meth. A* **654**, 432 (2011), [arXiv:1102.3876 \[hep-ex\]](#).
- [34] T. Chen and C. Guestrin, *Proceedings of the 22nd ACM SIGKDD International Conference on Knowledge Discovery and Data Mining KDD '16*, 785 (2016).
- [35] B. Efron, *The Annals of Statistics* **7**, 1 (1979).
- [36] K. G. Hayes, M. L. Perl, and B. Efron, *Phys. Rev. D* **39**, 274 (1989).
- [37] A. Hocker and V. Kartvelishvili, *Nucl. Instrum. Meth. A* **372**, 469 (1996), [arXiv:hep-ph/9509307](#).
- [38] T. Adye, in *Proceedings of the PHYSTAT 2011* (CERN, Geneva, 2011) [arXiv:1105.1160 \[physics.data-an\]](#).
- [39] See the supplemental material at the end of the paper.
- [40] B. O. Lange, M. Neubert, and G. Paz, *Phys. Rev. D* **72**, 073006 (2005), [arXiv:hep-ph/0504071](#).
- [41] K. Tackmann (BaBar), *Eur. Phys. J. A* **38**, 137 (2008), [arXiv:0801.2985 \[hep-ex\]](#).
- [42] J. P. Lees *et al.* (BaBar), *Phys. Rev. D* **95**, 072001 (2017), [arXiv:1611.05624 \[hep-ex\]](#).
- [43] O. Buchmuller and H. Flacher, *Phys. Rev. D* **73**, 073008 (2006), [arXiv:hep-ph/0507253](#).
- [44] M. Althoff *et al.* (TASSO Collaboration), *Z. Phys. C* **27**, 27 (1985).
- [45] W. Bartel *et al.* (JADE Collaboration), *Z. Phys. C* **20**, 187 (1983).

SUPPLEMENTAL MATERIAL

HEPDATA and Forward-Folding

The results will be made fully available in HEPData (<https://www.hepdata.net>), including the background subtracted yields, migration matrices, and efficiency curves. This will allow interested parties to also forward-fold $B \rightarrow X_u \ell^+ \nu_\ell$ theory predictions and directly compare such with the background subtracted Belle data.

Systematic Uncertainties

Figure 4 displays the systematic uncertainties of E_ℓ^B , M_X^2 , P_\pm shown as relative errors with respect to the measured differential branching fraction. The low E_ℓ^B region is dominated by uncertainties from the modeling of the inclusive $B \rightarrow X_u \ell^+ \nu_\ell$ and the background subtraction uncertainties. The endpoint of the E_ℓ^B spectrum is dominated by contributions from resonant $B \rightarrow X_u \ell^+ \nu_\ell$ decays. The systematic uncertainties for large M_X^2 are fully dominated by the background subtraction error. The systematic errors for P_- show three distinct regions: the intermediate region is dominated by the background subtraction uncertainties, whereas the low and high P_- region are dominated by exclusive and inclusive $B \rightarrow X_u \ell^+ \nu_\ell$ modeling uncertainties. The uncertainties at large P_+ values are fully dominated by the modeling of the inclusive parts of the $B \rightarrow X_u \ell^+ \nu_\ell$ hybrid.

Systematic uncertainties are consistently propagated through the entire analysis procedure, including the unfolding and efficiency correction. Tables II-VII provide a full summary of all the considered systematic uncertainties. A brief summary on the most significant uncertainties follows (note that they are evaluated in the same manner as described in Ref. [1]):

- The uncertainty on the tracking efficiency is evaluated by assigning an error of 0.35% per charged track on the $B \rightarrow X_u \ell^+ \nu_\ell$ signal side.
- The tagging calibration uncertainties are evaluated by producing different sets of calibration factors, which take into account the correlation structure from common systematic uncertainties and that individual channels and ranges of the output classifier are statistically independent. The uncertainty on the calibration factors is about 3.6% and only a negligible dependence on the studied kinematic distributions is observed.
- The uncertainties on the composition of the used $B \rightarrow X_u \ell^+ \nu_\ell$ MC is evaluated by variations of the $B \rightarrow \pi \ell^+ \nu_\ell$, $B \rightarrow \rho \ell^+ \nu_\ell$, $B \rightarrow \omega \ell^+ \nu_\ell$, $B \rightarrow \eta \ell^+ \nu_\ell$, $B \rightarrow \eta' \ell^+ \nu_\ell$ branching fractions and form factors. Semileptonic $B \rightarrow \pi \ell^+ \nu_\ell$ decays are simulated using the Bourrely-Caprini-Lellouch (BCL) parametrization [12] with form factor central values and uncertainties from the global fit carried out by Ref. [13]. The processes of $B \rightarrow \rho \ell^+ \nu_\ell$ and $B \rightarrow \omega \ell^+ \nu_\ell$ are modeled using the BCL form factor parametrization. We use the fit of Ref. [16], that combines the measurements of Refs. [18–20] with the light-cone sum rule predictions of Ref. [17] to determine a set of form factor central values and uncertainties. The processes of $B \rightarrow \eta \ell^+ \nu_\ell$ and $B \rightarrow \eta' \ell^+ \nu_\ell$ are modeled using the LCSR calculation of Ref. [15]. The uncertainty on non-resonant $B \rightarrow X_u \ell^+ \nu_\ell$ contributions in the used hybrid model is estimated by changing the underlying model from that of DFN [21] to that of BLNP [40]. In addition, the uncertainty on the used DFN parameters $m_b^{\text{KN}} = (4.66 \pm 0.04)$ GeV and $a^{\text{KN}} = 1.3 \pm 0.5$ from Ref. [43] are incorporated. For each of these variations, new hybrid weights are calculated to propagate the uncertainties into the full analysis procedure in a consistent way.
- The uncertainties of X_u fragmentation into $s\bar{s}$ quark pairs is evaluated by variations of the corresponding JETSET parameter γ_s [26]. We vary the $s\bar{s}$ production probability within $\gamma_s = 0.30 \pm 0.09$, with an uncertainty covering the range of the direct measurements of Refs. [44, 45] of $\gamma_s = 0.35 \pm 0.05$ and $\gamma_s = 0.27 \pm 0.06$.
- The X_u system of the non-resonant signal component is hadronized by JETSET into final states with two or more pions. We assign an uncertainty on the multiplicity modeling by changing the pion multiplicity of non-resonant $B \rightarrow X_u \ell^+ \nu_\ell$ to the distribution observed in data in the signal enriched region of $M_X < 1.7$ GeV, identical to the approach adopted in Ref. [1].
- The uncertainties on the modeling of $B \rightarrow D \ell^+ \nu_\ell$, $B \rightarrow D^* \ell^+ \nu_\ell$ and $B \rightarrow D^{**} \ell^+ \nu_\ell$ are evaluated by variations of the BGL parameters and heavy quark form factors within their uncertainties. The $B \rightarrow D \ell^+ \nu_\ell$ decays are modeled using the Boyd-Grinstein-Lebed (BGL) parametrization [27] with form factor central values and uncertainties taken from the fit in Ref. [30]. For $B \rightarrow D^* \ell^+ \nu_\ell$ we use the BGL implementation proposed

by Refs. [28, 29] with form factor central values and uncertainties from the fit to the measurement of Ref. [31]. Both backgrounds are normalized to the average branching fraction of Ref. [14] assuming isospin symmetry. Semileptonic $B \rightarrow D^{**} \ell^+ \nu_\ell$ decays with $D^{**} = \{D_0^*, D_1^*, D_1, D_2^*\}$ denoting the four orbitally excited charmed mesons are modeled using the heavy-quark-symmetry-based form factors proposed in Ref. [32]. In addition, the branching fraction uncertainties are included and the uncertainties on the $B \rightarrow X_c \ell^+ \nu_\ell$ gap branching fractions are taken to be large enough to account for the difference between the sum of all exclusive branching fractions measured and the inclusive branching fraction measured.

- The impact on the efficiency of the lepton- and hadron-identification uncertainties is evaluated by producing replicas of the simulated samples with new correction weights sampled from the measured corrections, that parametrize the difference between simulated and recorded collision event efficiencies on the identification efficiency as a function of the laboratory momentum and polar angle of the charged particle in question.
- The slow pion and K_S^0 reconstruction efficiencies are also evaluated using replicas of simulated samples, by producing sets of new correction weights, that parametrize the difference in the reconstruction efficiency between simulated and recorded collision event efficiencies.

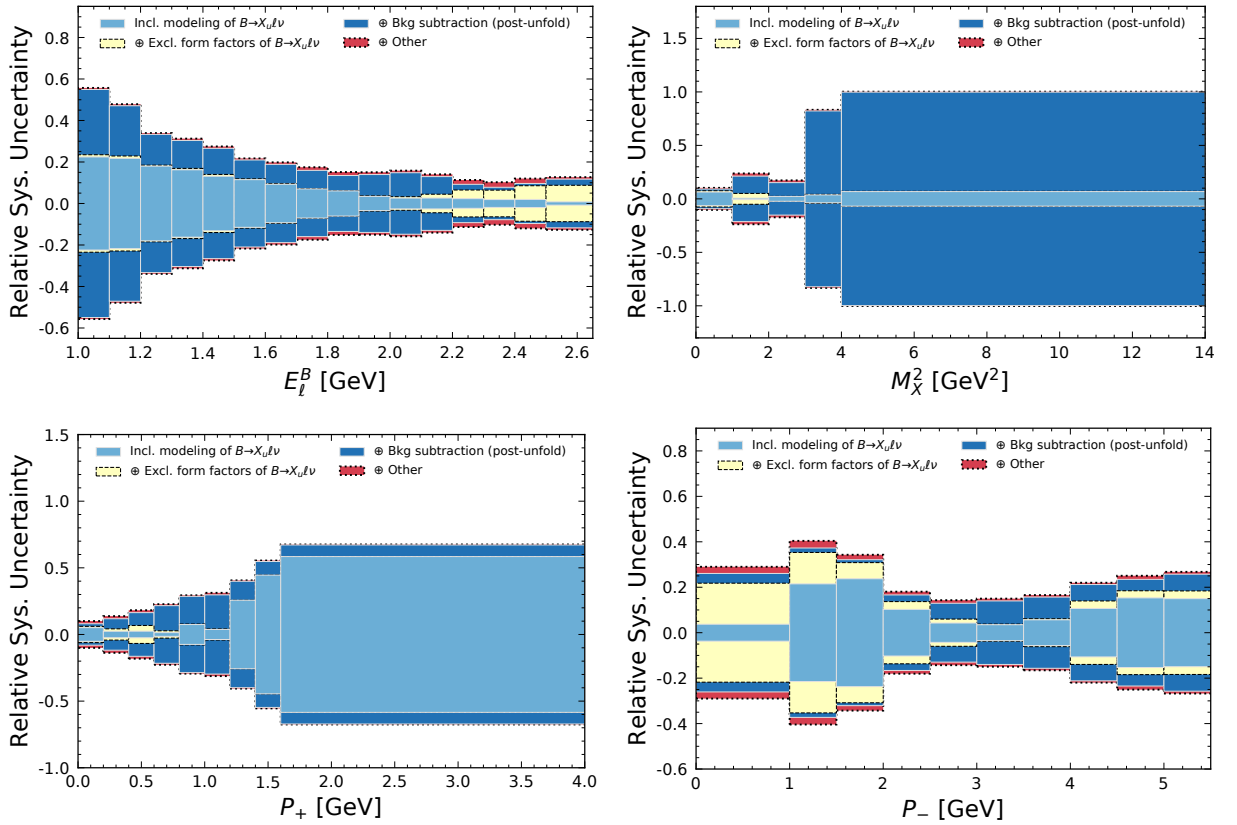


FIG. 4. The systematic uncertainties on the differential $B \rightarrow X_u \ell^+ \nu_\ell$ branching fractions as a function of E_ℓ^B , M_X^2 , and P_\pm are shown. They are separated into systematic uncertainties associated to the modeling of the inclusive and exclusive parts of the $B \rightarrow X_u \ell^+ \nu_\ell$ signal, the background subtraction, and other sources.

Migration Matrices

The migration matrices of all studied distributions, defined as the conditional probability

$$M_{ij} = P(\text{event reconstructed in bin } i | \text{event generated in bin } j), \quad (1)$$

M_X [GeV]	0-0.3	0.3-0.6	0.6-0.9	0.9-1.2	1.2-1.5	1.5-1.8	1.8-2.1	2.1-4.0
Tracking efficiency	0.55	0.56	0.82	0.86	0.95	1.05	1.15	1.19
Tagging calibration	3.69	3.69	3.65	3.64	3.64	3.57	3.79	3.66
Slow pion efficiency	0.00	0.07	0.04	0.05	0.04	0.04	0.06	0.04
K_S^0	0.04	0.05	0.04	0.02	0.04	0.03	0.02	0.05
e ID	0.72	0.83	0.74	0.69	0.73	0.74	0.94	1.22
μ ID	1.59	1.25	1.34	1.29	1.44	1.35	1.09	0.70
K/π ID	0.39	0.67	0.68	0.74	0.81	1.02	1.27	1.24
$\mathcal{B}(B \rightarrow X_{u\ell\nu})$	0.18	0.44	0.07	0.59	0.82	0.69	0.73	0.46
$\mathcal{B}(B \rightarrow \pi\ell\nu)$	0.42	0.45	0.45	0.14	0.05	0.04	0.05	0.05
$\mathcal{B}(B \rightarrow \rho\ell\nu)$	0.42	1.00	0.61	0.56	0.33	0.16	0.22	0.15
$\mathcal{B}(B \rightarrow \omega\ell\nu)$	0.42	0.39	0.65	0.12	0.11	0.06	0.11	0.10
$\mathcal{B}(B \rightarrow \eta\ell\nu)$	0.41	1.16	0.46	0.11	0.06	0.03	0.03	0.14
$\mathcal{B}(B \rightarrow \eta'\ell\nu)$	0.42	0.39	0.46	0.24	0.30	0.03	0.14	0.11
$B \rightarrow \pi\ell\nu$ FF	0.98	3.08	1.52	0.53	1.05	0.37	0.36	0.38
$B \rightarrow \rho\ell\nu$ FF	2.77	8.54	3.96	2.94	1.65	0.59	0.83	0.89
$B \rightarrow \omega\ell\nu$ FF	2.40	9.71	1.10	0.90	1.41	0.70	0.65	1.32
$B \rightarrow \eta\ell\nu$ FF	0.71	3.58	0.09	0.09	0.51	0.28	0.27	0.07
$B \rightarrow \eta'\ell\nu$ FF	0.69	3.65	0.16	0.27	0.48	0.29	0.32	0.15
Hybrid model	0.21	5.86	5.08	4.01	0.50	1.97	2.02	6.13
DFN parameters	0.18	3.66	1.01	1.38	1.64	0.87	0.50	1.35
γ_s	0.47	4.17	2.36	3.98	3.08	4.10	9.31	3.60
π^+ multiplicity modeling	0.57	0.42	0.45	4.15	7.98	4.78	3.98	2.34
$N_{B\bar{B}}$	1.25	1.25	1.25	1.25	1.25	1.25	1.25	1.25
Background subtraction	5.97	26.93	8.23	25.15	29.65	16.80	73.36	126.64
MC stat. (migration matrix)	4.04	11.22	3.54	6.85	4.30	4.71	6.85	8.22
Total syst. uncertainty	9.36	33.77	12.32	27.56	31.62	19.21	74.55	127.23
Total stat. uncertainty	11.11	32.64	10.77	24.99	21.88	16.54	46.24	66.76
Total uncertainty	14.53	46.97	16.36	37.20	38.45	25.35	87.73	143.68

TABLE II. The relative uncertainties (%) of the measured differential branching fraction of M_X are shown.

are shown in Figure 5. The binning of the measured distributions was chosen, such that the purity M_{ii} is at least 50%. The statistical uncertainty of the migration matrices due to the limited MC size is considered as a systematic uncertainty, cf. Tables II-VII.

Efficiency Correction Factors

The unfolded signal yields ν_i of a given bin i are corrected for selection efficiency, acceptance and phase-space effects, and normalized to the total number of recored B -meson pairs, $N_{B\bar{B}} = (771.58 \pm 9.78) \times 10^6$, to obtain differential branching fractions:

$$\Delta\mathcal{B}_i = \frac{1}{4N_{B\bar{B}}} \times \nu_i \times (\epsilon_{\text{tag}} \times \epsilon_{\text{sel}})^{-1} \times \epsilon_{\Delta\mathcal{B}(E_\ell^B > 1 \text{ GeV})}. \quad (2)$$

The factor of 4 is due to $N_{B\bar{B}}$ and that we average over electron and muon final states. Further, ϵ_{tag} and ϵ_{sel} denote the tagging and selection efficiencies, respectively, and $\epsilon_{\Delta\mathcal{B}(E_\ell^B > 1 \text{ GeV})}$ maps the branching fraction to the partial phase space with $E_\ell^B > 1 \text{ GeV}$ in the B rest frame. Figure 6 shows the product of $(\epsilon_{\text{tag}} \times \epsilon_{\text{sel}})^{-1} \times \epsilon_{\Delta\mathcal{B}(E_\ell^B > 1 \text{ GeV})}$ for all studied differential variables, including the full systematic uncertainties. The bottom panel shows the phase space acceptance $\epsilon_{\Delta\mathcal{B}(E_\ell^B > 1 \text{ GeV})}$.

M_X^2 [GeV ²]	0-1	1-2	2-3	3-4	4-14
Tracking efficiency	0.69	0.96	1.01	1.20	1.16
Tagging calibration	3.67	3.62	3.60	3.72	3.73
Slow pion efficiency	0.03	0.05	0.05	0.05	0.03
K_S^0	0.04	0.02	0.04	0.04	0.04
e ID	0.74	0.70	0.74	0.96	1.12
μ ID	1.42	1.33	1.37	0.99	0.89
K/π ID	0.55	0.89	0.92	1.22	1.24
$\mathcal{B}(B \rightarrow X_u \ell \nu)$	0.77	0.11	0.08	2.15	0.12
$\mathcal{B}(B \rightarrow \pi \ell \nu)$	0.67	0.43	0.07	0.23	0.04
$\mathcal{B}(B \rightarrow \rho \ell \nu)$	0.37	0.49	0.07	0.28	0.10
$\mathcal{B}(B \rightarrow \omega \ell \nu)$	0.45	0.07	0.03	0.16	0.05
$\mathcal{B}(B \rightarrow \eta \ell \nu)$	0.36	0.10	0.03	0.14	0.16
$\mathcal{B}(B \rightarrow \eta' \ell \nu)$	0.56	0.47	0.18	0.09	0.06
$B \rightarrow \pi \ell \nu$ FF	1.24	1.87	0.09	1.08	0.95
$B \rightarrow \rho \ell \nu$ FF	2.14	3.03	0.41	1.03	1.01
$B \rightarrow \omega \ell \nu$ FF	2.88	3.10	0.38	1.08	1.08
$B \rightarrow \eta \ell \nu$ FF	0.88	1.18	0.02	0.54	0.36
$B \rightarrow \eta' \ell \nu$ FF	0.91	1.30	0.03	0.53	0.49
Hybrid model	6.25	0.37	1.95	3.16	6.71
DFN parameters	1.25	0.56	1.18	1.90	1.13
γ_s	0.90	3.76	2.63	9.53	7.82
π^+ multiplicity	0.24	8.89	6.56	7.71	1.98
$N_{B\bar{B}}$	1.25	1.25	1.25	1.25	1.25
Background subtraction	4.86	20.19	14.45	81.67	99.28
MC stat. (migration matrix)	2.12	4.29	3.99	8.41	7.19
Total syst. uncertainty	10.30	23.76	17.29	83.27	100.22
Total stat. uncertainty	5.66	15.88	14.97	58.02	46.97
Total uncertainty	11.75	28.58	22.88	101.49	110.68

TABLE III. The relative uncertainties (%) of the measured differential branching fraction of M_X^2 are shown.

Experimental Correlations of the Differential Branching Fractions

The statistical and full experimental correlations of the measured distributions are shown in Figures 7 and 8. The statistical correlations were obtained using a bootstrapping procedure: ensembles of the selected data events after the initial selection were created and the full analysis was repeated (binned likelihood fit in M_X , background subtraction in the variable of interest, unfolding, efficiency correction). From the obtained central values of these ensembles, the statistical correlations between observables were estimated using the Pearson correlation coefficient.

Total Partial Branching Fractions and Comparison to Ref. [1]

The left panel of Figure 9 shows the partial branching fractions for $E_\ell^B > 1$ GeV as calculated when summing the individual bins of the differential measurements of M_X , M_X^2 , E_ℓ^B , q^2 , and P_\pm . The values agree with the value reported in Ref. [1], which uses the same analysis strategy but less strict selection criteria. To further study the compatibility, we evaluate the ratios of the partial branching fractions with respect to the partial branching fraction obtained from the M_X distribution, taking into account the full statistical and systematic correlations. We find good overall agreement and the largest discrepancy is from the ratio of P_+ , which agrees with unity to within 0.9 standard deviation. The right panel of Figure 9 shows the experimental correlation of the partial branching fractions obtained by summing the individually measured bins.

q^2 [GeV ²]	0-2	2-4	4-6	6-8	8-10	10-12	12-14	14-16	16-18	18-20	20-22	22-26.5
Tracking efficiency	0.93	0.95	0.94	0.90	0.89	0.87	0.82	0.75	0.72	0.67	0.55	0.57
Tagging calibration	3.58	3.69	3.71	3.69	3.65	3.63	3.63	3.64	3.64	3.73	3.86	3.76
Slow pion efficiency	0.02	0.03	0.04	0.03	0.04	0.04	0.04	0.04	0.04	0.06	0.09	0.07
K_S^0	0.03	0.03	0.04	0.03	0.03	0.04	0.04	0.04	0.03	0.03	0.04	0.04
eID	0.79	0.77	0.77	0.75	0.74	0.66	0.69	0.83	0.87	0.83	0.82	0.79
μ ID	1.39	1.26	1.24	1.32	1.34	1.46	1.45	1.39	1.33	1.52	1.64	1.47
K/π ID	0.85	0.96	0.93	0.83	0.79	0.77	0.70	0.65	0.53	0.35	0.20	0.22
$\mathcal{B}(B \rightarrow X_u \ell \nu)$	1.26	1.01	0.75	0.54	0.42	0.01	0.56	1.06	2.01	1.47	0.64	0.45
$\mathcal{B}(B \rightarrow \pi \ell \nu)$	1.21	0.95	0.77	0.59	0.27	0.36	1.25	2.93	5.10	6.53	5.64	5.65
$\mathcal{B}(B \rightarrow \rho \ell \nu)$	1.14	0.96	0.89	0.64	0.39	0.59	1.37	3.06	5.13	6.55	5.62	5.64
$\mathcal{B}(B \rightarrow \omega \ell \nu)$	1.13	0.92	0.74	0.52	0.21	0.32	1.23	2.92	5.09	6.53	5.62	5.61
$\mathcal{B}(B \rightarrow \eta \ell \nu)$	1.14	0.93	0.74	0.54	0.26	0.35	1.23	2.91	5.09	6.53	5.62	5.61
$\mathcal{B}(B \rightarrow \eta' \ell \nu)$	1.13	0.94	0.74	0.53	0.22	0.33	1.23	2.92	5.08	6.53	5.62	5.61
$B \rightarrow \pi \ell \nu$ FF	2.60	3.00	2.38	1.25	0.38	0.83	2.12	4.39	3.83	2.07	5.51	2.63
$B \rightarrow \rho \ell \nu$ FF	5.05	5.44	4.29	2.36	1.29	1.18	2.46	7.53	10.45	7.01	15.88	8.74
$B \rightarrow \omega \ell \nu$ FF	6.69	8.65	5.85	2.92	1.07	1.19	4.27	9.92	13.29	16.85	20.29	9.44
$B \rightarrow \eta \ell \nu$ FF	2.35	2.53	1.67	0.85	0.34	0.35	1.41	2.76	2.80	2.76	6.99	3.00
$B \rightarrow \eta' \ell \nu$ FF	2.42	2.62	1.74	0.92	0.38	0.39	1.34	2.78	3.20	2.90	6.53	3.30
Hybrid model	16.17	16.41	9.91	2.71	3.62	4.69	9.82	12.48	15.53	11.75	23.34	5.45
DFN parameters	6.01	6.43	4.78	3.86	4.12	3.19	2.03	1.44	1.10	1.01	3.26	1.01
γ_s	6.28	4.39	1.39	1.41	1.52	3.14	0.43	0.07	1.98	1.99	0.47	1.09
π^+ multiplicity	2.74	3.08	2.85	2.18	3.18	4.00	3.09	0.10	0.14	0.07	1.41	0.42
$N_{B\bar{B}}$	1.25	1.25	1.25	1.25	1.25	1.25	1.25	1.25	1.25	1.25	1.25	1.25
Background subtraction	16.66	16.89	16.52	13.79	12.22	11.30	10.67	11.54	9.77	9.14	10.18	12.96
MC stat. (migration matrix)	2.94	3.15	2.37	2.29	2.56	2.87	2.69	3.62	3.40	3.81	7.33	7.81
Total syst. uncertainty	27.32	28.03	22.28	16.20	14.86	14.73	17.05	23.60	28.71	28.79	40.98	25.11
Total stat. uncertainty	16.71	13.67	13.05	11.61	12.26	12.87	12.45	13.30	11.96	12.12	15.69	19.97
Total uncertainty	32.02	31.19	25.82	19.93	19.26	19.56	21.11	27.09	31.10	31.23	43.88	32.08

TABLE IV. The relative uncertainties (%) of the measured differential branching fraction of q^2 are shown.

E_ℓ^P [GeV]	1.0-1.1	1.1-1.2	1.2-1.3	1.3-1.4	1.4-1.5	1.5-1.6	1.6-1.7	1.7-1.8	1.8-1.9	1.9-2.0	2.0-2.1	2.1-2.2	2.2-2.3	2.3-2.4	2.4-2.5	2.5-2.65
Tracking efficiency	0.39	0.39	0.39	0.39	0.39	0.38	0.39	0.39	0.39	0.39	0.38	0.38	0.38	0.38	0.38	0.38
Tagging calibration	3.75	3.71	3.67	3.65	3.63	3.67	3.69	3.68	3.69	3.71	3.67	3.66	3.66	3.67	3.73	3.74
Slow pion efficiency	0.04	0.04	0.04	0.04	0.04	0.05	0.06	0.06	0.07	0.07	0.07	0.08	0.08	0.08	0.07	0.06
K_S^0	0.04	0.04	0.04	0.04	0.04	0.04	0.04	0.04	0.04	0.04	0.04	0.04	0.04	0.04	0.03	0.04
e ID	1.34	1.20	0.93	0.79	0.71	0.70	0.69	0.70	0.72	0.71	0.73	0.76	0.78	0.76	0.78	0.79
μ ID	1.15	1.17	1.29	1.35	1.36	1.37	1.37	1.36	1.38	1.41	1.43	1.46	1.43	1.52	1.53	1.43
K/π ID	0.90	0.91	0.83	0.83	0.87	0.88	0.95	0.91	0.85	0.82	0.75	0.71	0.67	0.66	0.57	0.56
$\mathcal{B}(B \rightarrow X_u \ell \nu)$	1.12	0.81	1.12	0.82	0.44	1.01	0.78	0.57	0.74	0.52	0.52	0.49	0.04	1.31	1.18	0.16
$\mathcal{B}(B \rightarrow \pi \ell \nu)$	0.69	0.66	0.64	0.60	0.55	0.45	0.35	0.27	0.23	0.29	0.41	0.71	1.22	1.97	2.14	0.85
$\mathcal{B}(B \rightarrow \rho \ell \nu)$	0.65	0.62	0.66	0.67	0.69	0.55	0.42	0.33	0.32	0.32	0.51	0.75	1.26	2.08	2.19	0.86
$\mathcal{B}(B \rightarrow \omega \ell \nu)$	0.64	0.61	0.57	0.52	0.47	0.39	0.30	0.19	0.04	0.14	0.37	0.69	1.19	1.95	2.12	0.85
$\mathcal{B}(B \rightarrow \eta \ell \nu)$	0.64	0.61	0.57	0.53	0.47	0.39	0.31	0.21	0.07	0.15	0.36	0.69	1.19	1.95	2.11	0.85
$\mathcal{B}(B \rightarrow \eta' \ell \nu)$	0.64	0.61	0.57	0.52	0.46	0.40	0.32	0.22	0.10	0.18	0.38	0.69	1.19	1.95	2.11	0.85
$B \rightarrow \pi \ell \nu$ FF	1.61	1.53	0.94	1.26	1.39	1.05	0.72	0.30	0.16	0.28	0.48	0.82	1.20	0.92	1.94	2.61
$B \rightarrow \rho \ell \nu$ FF	3.62	3.56	2.16	2.63	2.78	1.86	1.52	0.86	0.40	0.57	1.25	2.02	3.36	3.19	4.01	4.55
$B \rightarrow \omega \ell \nu$ FF	5.29	5.52	3.01	3.38	3.32	1.94	1.73	1.00	0.58	1.20	1.38	2.65	4.57	4.97	6.55	6.29
$B \rightarrow \eta \ell \nu$ FF	1.69	1.62	0.92	1.10	1.17	0.77	0.61	0.28	0.12	0.21	0.37	0.83	1.31	1.06	1.79	2.09
$B \rightarrow \eta' \ell \nu$ FF	1.56	1.58	0.95	1.16	1.20	0.80	0.65	0.33	0.09	0.23	0.33	0.77	1.21	0.99	1.89	2.22
Hybrid model	21.68	21.05	17.09	15.34	12.37	10.28	8.24	5.84	4.90	1.21	0.72	1.68	1.93	0.89	1.29	0.43
DFN parameters	5.74	5.52	5.69	5.31	4.41	5.12	4.26	3.88	3.55	3.20	2.50	2.02	1.30	1.67	1.45	0.66
γ_s	7.06	6.26	3.45	5.13	4.76	0.87	1.64	4.12	3.92	1.72	1.50	0.62	3.52	1.34	2.59	1.14
π^+ multiplicity	3.19	3.35	2.89	2.65	2.55	3.41	3.86	3.83	3.63	3.13	3.06	2.86	2.28	1.62	1.11	0.23
$N_{B\bar{B}}$	1.25	1.25	1.25	1.25	1.25	1.25	1.25	1.25	1.25	1.25	1.25	1.25	1.25	1.25	1.25	1.25
Background subtraction	49.32	40.78	27.56	25.05	22.39	17.20	16.10	14.09	11.89	13.35	14.39	12.03	6.05	3.85	3.85	6.54
MC stat. (migration matrix)	5.92	5.53	3.03	3.17	3.00	1.54	1.91	2.28	1.74	1.62	1.38	1.82	2.56	2.19	2.26	4.22
Total syst. uncertainty	55.70	47.86	33.93	31.26	27.48	21.73	19.82	17.48	15.15	15.05	15.83	14.06	11.34	10.26	12.01	12.70
Total stat. uncertainty	54.34	39.47	23.05	19.69	17.06	13.07	13.04	12.21	9.40	8.18	7.60	7.47	6.95	6.08	6.96	11.22
Total uncertainty	77.82	62.03	41.02	36.94	32.34	25.36	23.73	21.32	17.82	17.13	17.56	15.92	13.30	11.92	13.88	16.94

TABLE V. The relative uncertainties (%) of the measured differential branching fraction of E_ℓ^P are shown.

P_+ [GeV]	0-0.2	0.2-0.4	0.4-0.6	0.6-0.8	0.8-1.0	1.0-1.2	1.2-1.4	1.4-1.6	1.6-4.0
Tracking efficiency	0.65	0.87	0.95	1.03	1.09	1.11	1.09	1.06	1.05
Tagging calibration	3.69	3.59	3.69	3.64	3.63	3.64	3.68	3.66	3.65
Slow pion efficiency	0.01	0.06	0.04	0.04	0.05	0.05	0.04	0.04	0.04
K_S^0	0.04	0.03	0.04	0.03	0.03	0.03	0.03	0.04	0.04
eID	0.70	0.79	0.77	0.74	0.77	0.87	0.91	0.89	0.89
μ ID	1.48	1.29	1.29	1.35	1.34	1.24	1.22	1.21	1.19
$K\pi$ ID	0.56	0.74	0.85	0.94	1.06	1.08	1.02	0.96	0.93
$\mathcal{B}(B \rightarrow X_u \ell \nu)$	0.67	0.66	1.45	1.22	0.31	0.59	0.42	1.28	1.62
$\mathcal{B}(B \rightarrow \pi \ell \nu)$	1.84	1.70	0.49	0.08	0.05	0.04	0.04	0.09	0.12
$\mathcal{B}(B \rightarrow \rho \ell \nu)$	1.69	2.03	0.52	0.39	0.14	0.07	0.09	0.06	0.06
$\mathcal{B}(B \rightarrow \omega \ell \nu)$	1.73	1.68	0.43	0.19	0.02	0.04	0.03	0.08	0.10
$\mathcal{B}(B \rightarrow \eta \ell \nu)$	1.67	1.68	0.42	0.08	0.01	0.04	0.04	0.04	0.05
$\mathcal{B}(B \rightarrow \eta' \ell \nu)$	1.68	1.68	0.41	0.12	0.05	0.02	0.03	0.04	0.05
$B \rightarrow \pi \ell \nu$ FF	0.73	0.32	1.54	0.55	1.23	0.74	0.03	0.36	0.54
$B \rightarrow \rho \ell \nu$ FF	2.40	2.19	5.04	2.14	1.33	1.32	0.28	0.58	0.93
$B \rightarrow \omega \ell \nu$ FF	1.96	2.66	3.29	0.75	1.40	0.87	0.12	0.67	0.93
$B \rightarrow \eta \ell \nu$ FF	0.69	0.19	0.62	0.31	0.59	0.33	0.01	0.18	0.26
$B \rightarrow \eta' \ell \nu$ FF	0.59	0.03	0.61	0.44	0.68	0.35	0.01	0.18	0.26
Hybrid model	4.74	2.04	1.68	0.84	7.24	3.10	25.53	43.81	55.28
DFN parameters	1.92	1.30	1.82	1.10	1.74	2.15	2.87	8.00	19.00
γ_s	1.69	2.79	3.23	2.81	4.60	8.56	5.83	7.64	4.77
π^+ multiplicity	0.24	2.94	5.47	4.58	2.04	0.23	0.57	1.40	1.74
$N_{B\bar{B}}$	1.25	1.25	1.25	1.25	1.25	1.25	1.25	1.25	1.25
Background subtraction	4.68	10.27	14.48	21.22	27.32	29.13	30.15	31.37	32.57
MC stat. (migration matrix)	2.42	4.01	3.60	3.06	3.33	4.07	4.95	5.24	5.53
Total syst. uncertainty	10.08	13.78	18.19	22.73	29.39	31.24	40.59	55.47	67.51
Total stat. uncertainty	6.86	10.89	13.64	16.39	16.51	16.77	22.05	25.67	27.62
Total uncertainty	12.20	17.56	22.74	28.03	33.71	35.46	46.19	61.12	72.94

TABLE VI. The relative uncertainties (%) of the measured differential branching fraction of P_+ are shown.

P_- [GeV]	0-1.0	1.0-1.5	1.5-2.0	2.0-2.5	2.5-3.0	3.0-3.5	3.5-4.0	4.0-4.5	4.5-5.0	5.0-5.5
Tracking efficiency	0.61	0.62	0.73	0.80	0.84	0.88	0.89	0.92	0.92	0.91
Tagging calibration	3.75	3.77	3.67	3.64	3.59	3.63	3.72	3.72	3.65	3.59
Slow pion efficiency	0.06	0.06	0.04	0.04	0.04	0.04	0.03	0.03	0.03	0.02
K_S^0	0.03	0.03	0.03	0.04	0.03	0.03	0.03	0.04	0.03	0.03
e ID	0.87	0.84	0.78	0.76	0.72	0.74	0.74	0.73	0.76	0.77
μ ID	1.38	1.50	1.47	1.39	1.37	1.42	1.31	1.25	1.32	1.42
$K\pi$ ID	0.23	0.25	0.47	0.69	0.78	0.77	0.83	0.90	0.88	0.86
$\mathcal{B}(B \rightarrow X_u \ell \nu)$	0.40	1.49	2.97	0.22	0.33	0.02	0.47	0.44	0.93	1.03
$\mathcal{B}(B \rightarrow \pi \ell \nu)$	5.22	6.42	4.64	2.35	0.93	0.21	0.50	0.84	1.16	1.41
$\mathcal{B}(B \rightarrow \rho \ell \nu)$	5.21	6.43	4.71	2.39	1.03	0.59	0.57	1.02	1.13	1.32
$\mathcal{B}(B \rightarrow \omega \ell \nu)$	5.21	6.40	4.62	2.33	0.91	0.10	0.42	0.78	1.10	1.32
$\mathcal{B}(B \rightarrow \eta \ell \nu)$	5.21	6.40	4.62	2.33	0.91	0.17	0.44	0.79	1.11	1.33
$\mathcal{B}(B \rightarrow \eta' \ell \nu)$	5.21	6.39	4.62	2.33	0.91	0.10	0.42	0.79	1.11	1.32
$B \rightarrow \pi \ell \nu$ FF	3.65	4.49	5.03	2.13	1.59	0.58	0.68	2.55	2.88	2.75
$B \rightarrow \rho \ell \nu$ FF	12.44	13.45	11.09	4.09	1.85	1.10	1.64	4.65	5.04	5.86
$B \rightarrow \omega \ell \nu$ FF	16.21	23.12	14.35	7.37	3.15	0.62	1.49	6.77	7.79	7.59
$B \rightarrow \eta \ell \nu$ FF	3.44	4.69	3.99	1.87	1.02	0.23	0.39	1.94	2.35	2.65
$B \rightarrow \eta' \ell \nu$ FF	4.25	5.23	4.28	1.79	0.95	0.24	0.39	1.99	2.45	2.74
Hybrid model	3.03	21.43	23.71	9.77	3.11	1.27	3.35	9.53	14.19	13.85
DFN parameters	2.17	1.59	1.12	3.11	2.90	3.27	4.57	4.77	5.76	5.68
γ_s	2.60	4.18	3.11	0.56	0.90	0.31	1.03	1.01	6.43	4.42
π^+ multiplicity	0.27	0.51	0.03	1.76	3.66	3.16	2.67	3.22	3.10	2.52
$N_{B\bar{B}}$	1.25	1.25	1.25	1.25	1.25	1.25	1.25	1.25	1.25	1.25
Background subtraction	13.11	10.18	8.43	9.12	11.20	13.27	14.29	15.73	14.29	17.77
MC stat. (migration matrix)	5.75	6.25	2.94	2.37	2.54	2.21	1.92	2.47	2.50	2.90
Total syst. uncertainty	29.00	40.42	34.30	18.05	14.30	14.98	16.56	21.98	25.06	26.78
Total stat. uncertainty	18.64	13.81	10.43	10.61	12.17	13.20	12.34	12.69	12.47	19.72
Total uncertainty	34.48	42.71	35.84	20.94	18.78	19.97	20.65	25.39	27.99	33.26

TABLE VII. The relative uncertainties (%) of the measured differential branching fraction of P_- are shown.

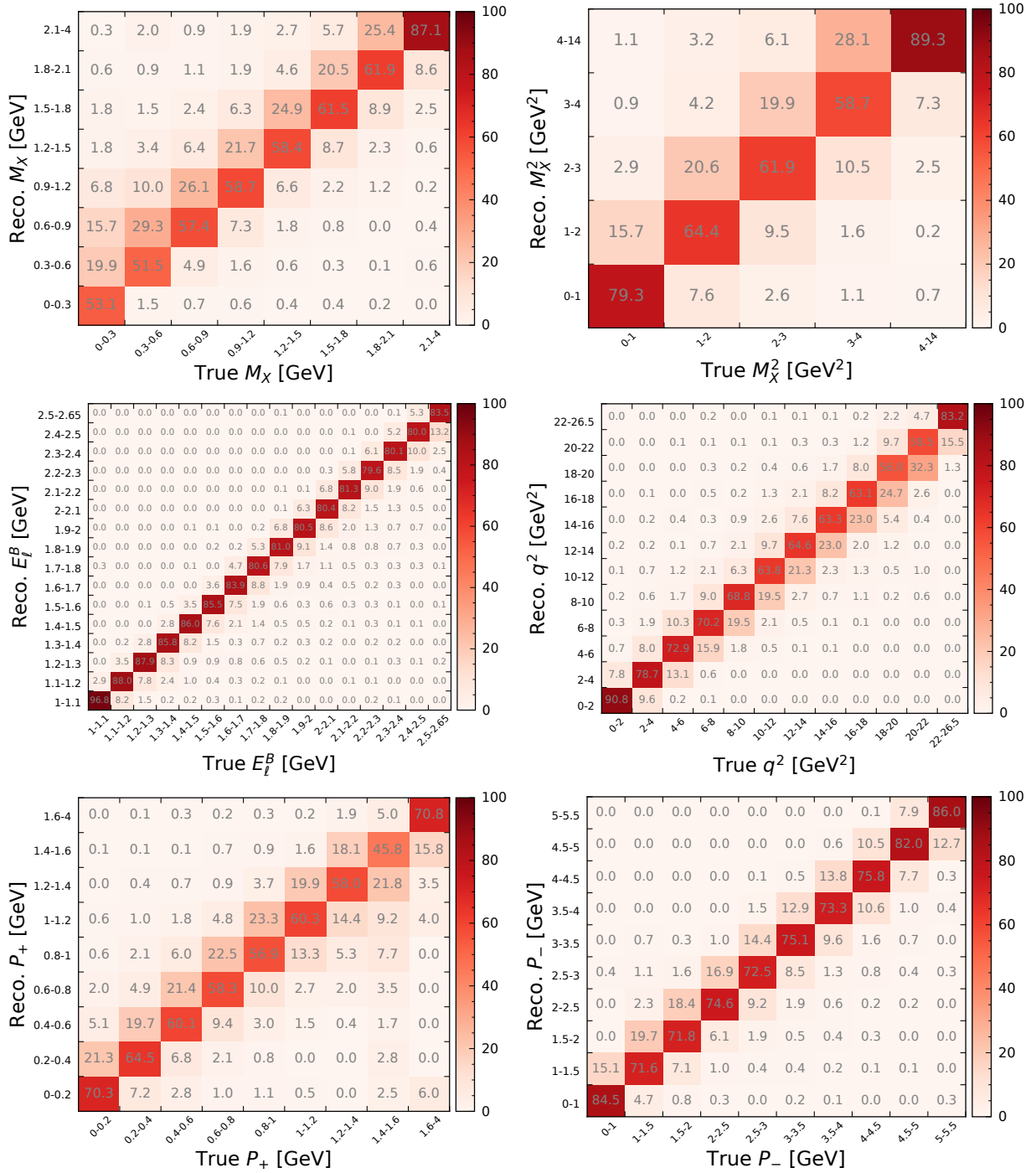


FIG. 5. The migration matrices for all studied variables are shown.

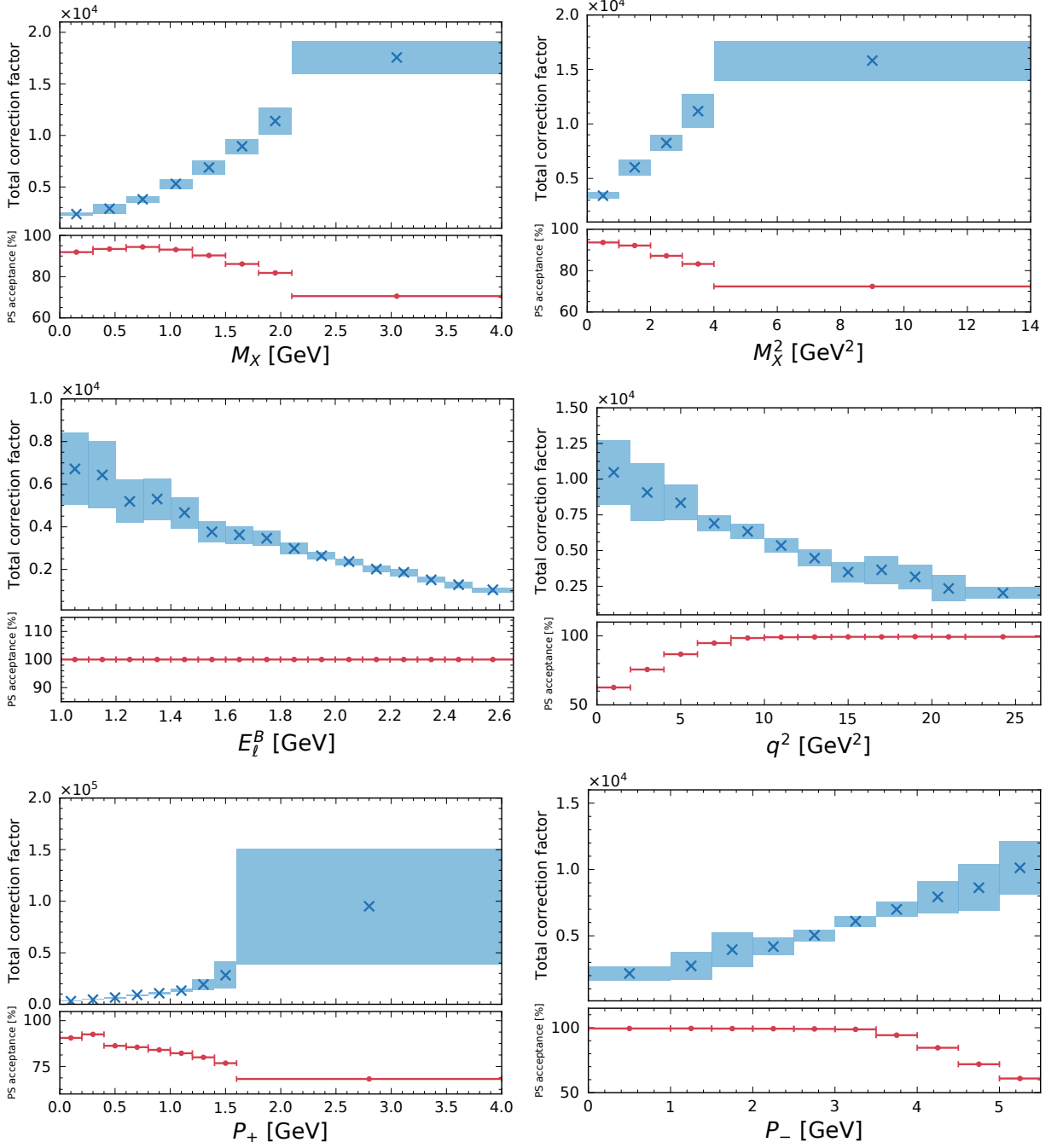


FIG. 6. The correction factors $(\epsilon_{\text{tag}} \times \epsilon_{\text{sel}})^{-1} \times \epsilon_{\Delta B(E_\ell^B > 1 \text{ GeV})}$ (blue) and phase space acceptance factor $\epsilon_{\Delta B(E_\ell^B > 1 \text{ GeV})}$ (red) are shown. The colored band of the total correction factor shows the full systematic uncertainty.

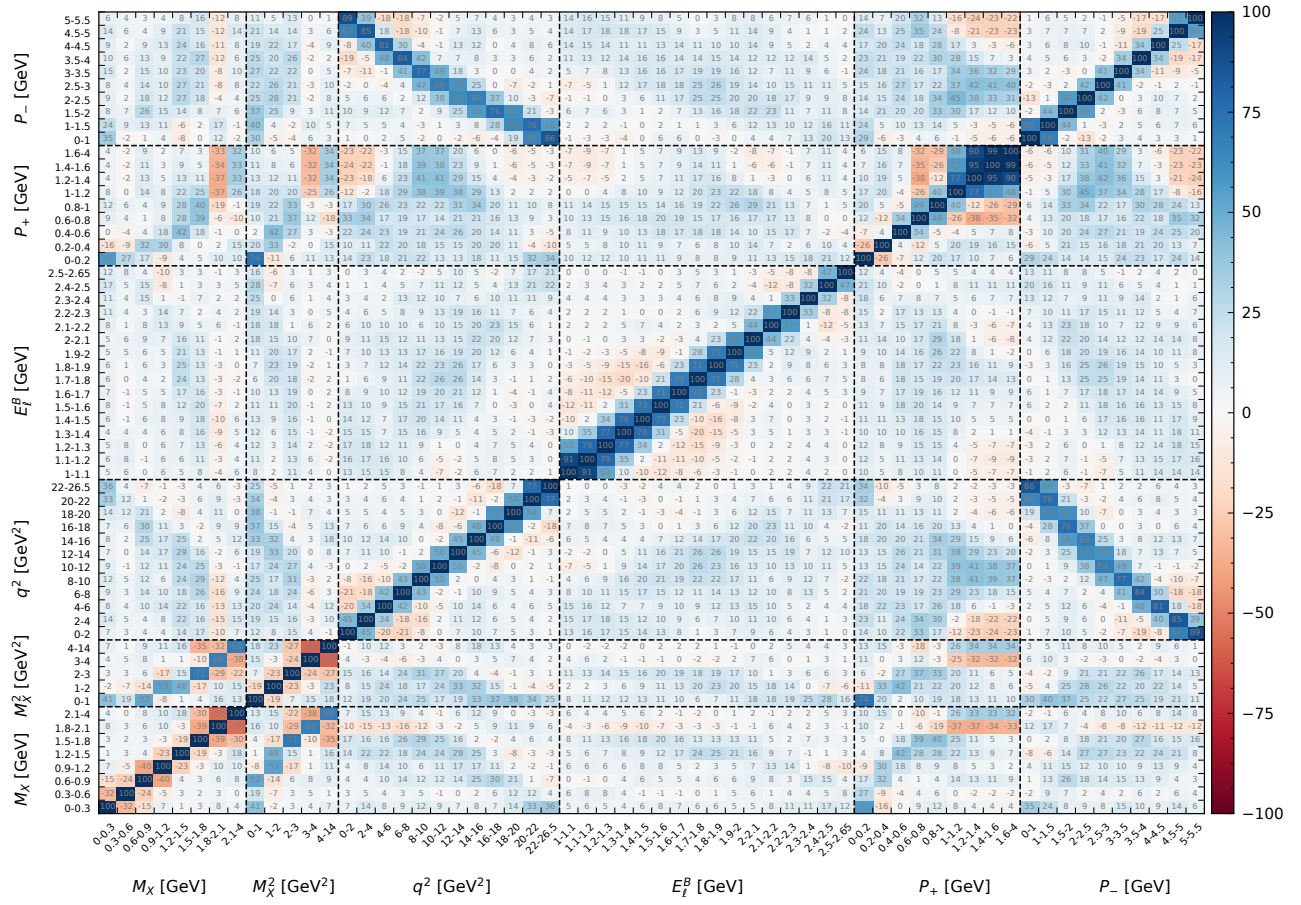


FIG. 7. The statistical correlations of the differential branching fractions are shown.

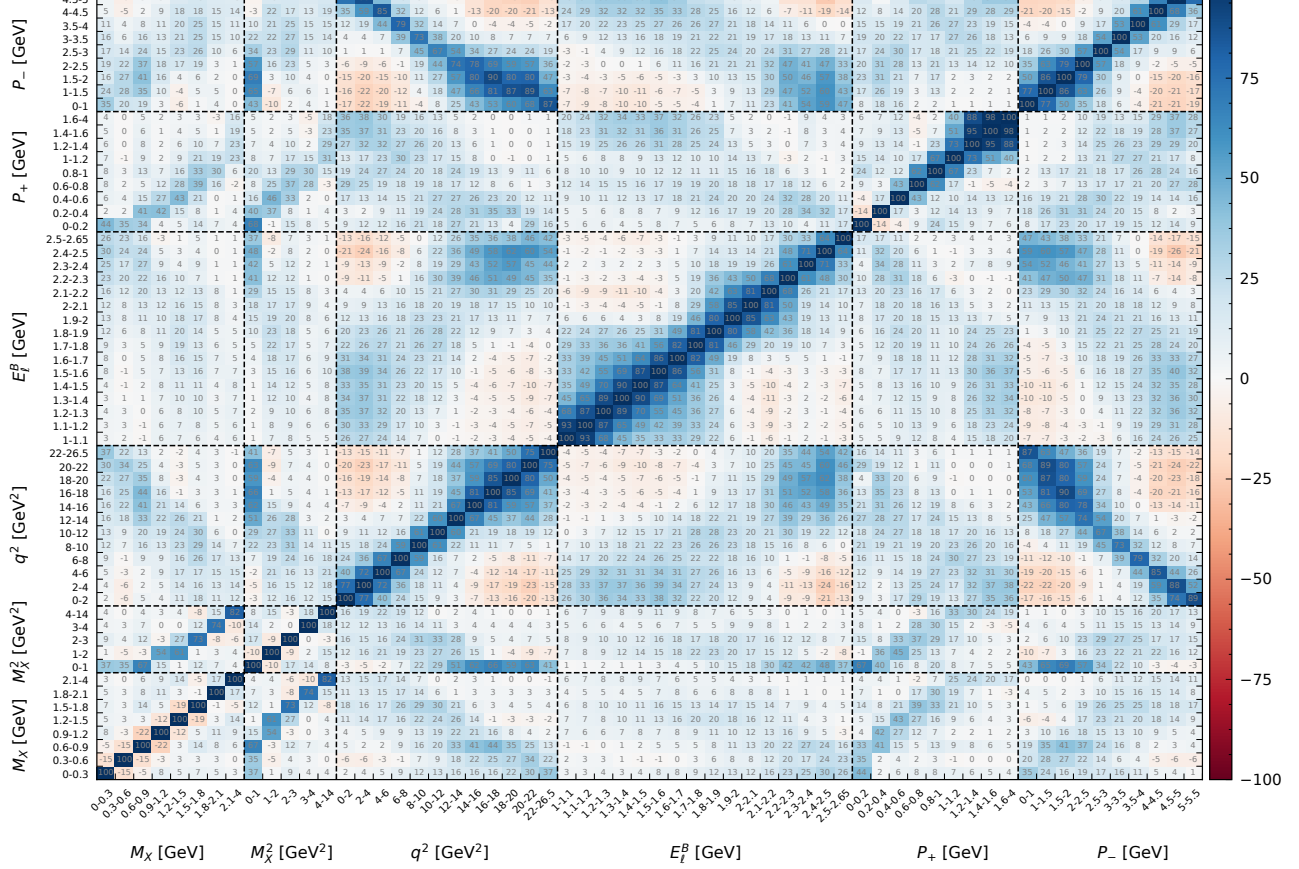


FIG. 8. The full experimental (statistical and systematical) correlations of the differential branching fractions are shown.

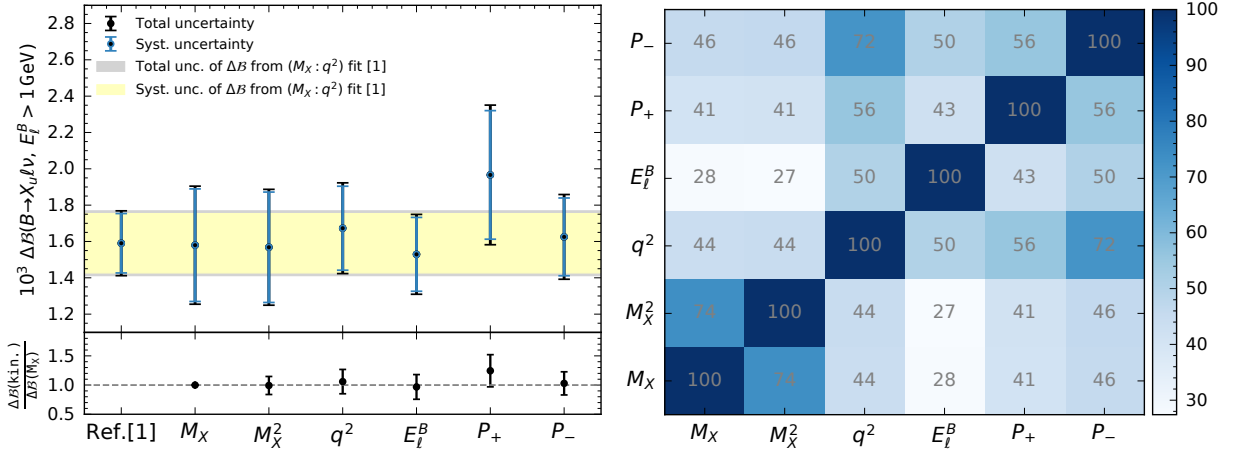


FIG. 9. (Left) The total partial branching fraction with $E_l^B > 1$ GeV as calculated by each differential measurement is compared to the result of Ref. [1], which is based on the 2D fit of $M_X : q^2$ and obtained with a looser selection. The ratio compares the total partial branching fractions to the result obtained by summing the measured M_X distribution and the uncertainty takes into account the full statistical and systematic correlations between the different results. (Right) The full experimental correlations between the total partial branching fractions from summing the individual bins are shown.